

Transitional millisecond pulsars

Alessandro Papitto & Domitilla de Martino

Abstract Millisecond pulsars in tight binaries have recently opened new challenges in our understanding of physical processes governing the evolution of binaries and the interaction between astrophysical plasma and electromagnetic fields. Transitional systems that showed changes from rotation-powered to accretion powered states and vice versa have bridged the populations of radio and accreting millisecond pulsars, eventually demonstrating the tight evolutionary link envisaged by the recycling scenario. A decade of discoveries and theoretical efforts have just grasped the complex phenomenology of transitional millisecond pulsars from the radio to the gamma-ray band. This review summarises the main properties of the three transitional millisecond pulsars discovered so far, as well as of candidates and related systems, discussing the various models proposed to cope with the multifaceted behaviour.

1 Introduction

The observation of dramatic changes of state over a few weeks is what makes *transitional* a millisecond pulsar (MSP) in a binary system. These sources experience transitions from a rotation-powered regime, in which they behave like radio pulsars whose wind prevents the in-fall of the matter lost by the low-mass companion, to a regime in which they accrete and emit intense high-energy radiation like X-ray binary systems, and vice versa. During the transitions the luminosity changes by at least an order of magnitude, likely due to variations in the mass inflow rate. The discovery of transitional millisecond pulsars (tMSPs in the following) has been a key achievement

Alessandro Papitto

INAF – Osservatorio Astronomico di Roma, via di Frascati 33, I-00078 Monte Porzio Catone (Roma), Italy, e-mail: alessandro.papitto@inaf.it

Domitilla de Martino

INAF – Osservatorio Astronomico di Capodimonte, Salita Moiariello 16, I-80131 Napoli, Italy, e-mail: domitilla.demartino@inaf.it

in the investigation of the evolution of MSPs. The recycling scenario developed in the early 1980s had postulated that radio MSPs were spun up in a previous Gyr-long phase of mass accretion [1, 2, 3, 4]. It implied that these fast-spinning neutron stars (NSs) were descendants of low-mass (donor mass $< 1 M_{\odot}$) X-ray binaries (LMXBs). The discovery of radio MSPs in globular clusters [5] and of accreting MSPs (AMXPs) in a handful of X-ray transients [6] underpinned this theory. Eventually, in 2009 a radio MSP binary was recognised to have been previously surrounded by an accretion disc [7]. A few years later, the same binary and two more systems were surprisingly found to switch back and forth accretion and rotation-powered regimes over much shorter timescales than the secular recycling binary evolution [8, 9, 10]. Whether these MSPs represent an intermediate evolutionary stage before they end as radio pulsars that completely devour their companions, or rather experience a distinct evolutionary path, has still to be assessed. Certainly, they have provided us with a unique occasion to observe the different possible outcomes of the interaction between a quickly spinning magnetised NS and plasma lost by a companion star as they unfold over timescales accessible to the human life.

TMSPs bridge a few classes of MSPs (see Sec. 2). The interplay between the gravitational pull exerted by the NS on the mass lost by the companion and the outward pressure of the pulsar wind determines whether an MSP behaves either as a rotation or as an accretion-powered source (see Sec. 3). As of June 2020, we currently know three transitional MSPs (see Sec. 4). They have shown radio pulsar states (Sec. 5.1), a bright accretion outburst in one of them (Sec. 5.2), but also an enigmatic X-ray *sub-luminous* disc state, which gave us a brand new view of how LMXBs may behave at low mass accretion rates (Sec. 5.3). The properties of tMSPs are so peculiar that they are key signatures to identify candidates that will likely perform a transition in the future (Sec. 5.4). Like in many cases, the discovery of tMSPs raised far more questions than it answered. What makes a system transitional? Are all MSPs in binaries with an orbital period shorter than a day (both accreting and eclipsing ones) transitional? How does the pulsar magnetic field interact with the in-flowing gas? Are the rotation and accretion powered regimes mutually exclusive, or do we rather see them mixed in the sub-luminous state? In Sec. 6 we discuss current models attempting to explain the enigmatic behaviour of these MSPs.

2 The population of millisecond pulsar binaries

As of June 2020, we know 20 accreting and 471 rotation-powered MSPs, here defined by a spin period < 30 ms. Fig. 1 shows the observed binary characteristics.

AMXPs are all found in X-ray transients, which undergo occasional outbursts reaching an X-ray luminosity up to $\sim 10^{36} - 10^{38} \text{ erg s}^{-1}$, interleaved by long periods of quiescence ($L_X \sim 10^{31} - 10^{32} \text{ erg s}^{-1}$; see [11, 12] for reviews). They are harboured in tight ($P_{orb} < 1$ day) binary systems (see orange symbols in Fig. 1), and half of them showed thermonuclear type-I bursts. Only IGR J18245-2452 has been also detected as a radio pulsar in quiescence, so far.

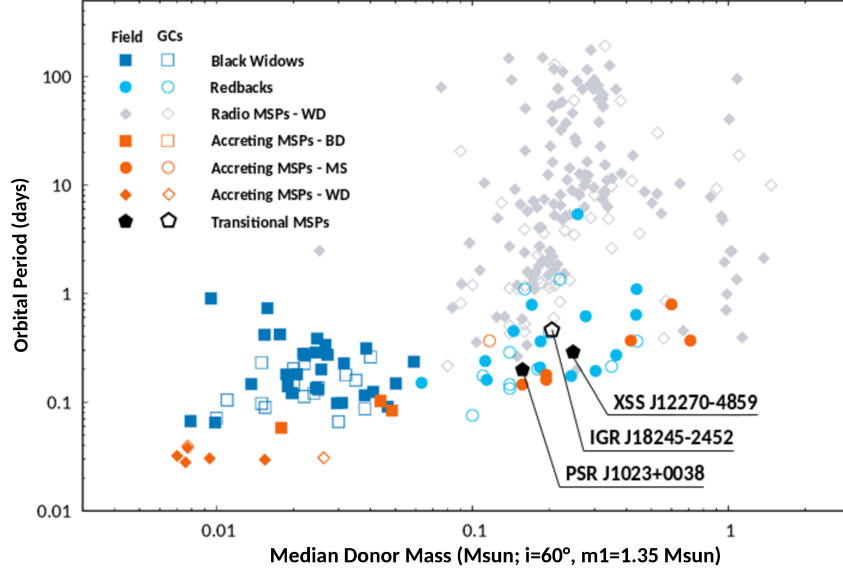


Fig. 1: Orbital period and median mass (evaluated from the pulsar timing parameters assuming an inclination of 60° and an NS mass of $1.35 M_\odot$) of black widows (blue squares), redbacks (cyan circles), non-interacting radio MSPs with a white dwarf companion (grey diamonds), AMXPs (orange symbols with shape depending on the donor type, squares for brown dwarfs, circles for main-sequence stars and diamonds for white dwarfs) and tMSPs (black pentagons). Filled and hollow symbols mark sources found in the Galactic field and globular clusters, respectively.

Rotation-powered radio MSPs are much more numerous. They amount to about 314 in the Galactic field¹ and 157 in 30 globular clusters². Here, we mainly address the ~ 100 MSPs in compact binaries ($P_{orb} < 1$ day), most of which show irregular radio eclipses due to the presence of intrabinary material. Dubbed "*spiders*" [13, 14], these binaries include "*black widows*" with very low-mass companions (defined by $< 0.06 M_\odot$) and "*redbacks*" with a hydrogen-rich secondary with a minimum mass of at least $\approx 0.1 M_\odot$ (see Fig. 1). When rotation powered, the three known tMSPs are redbacks. Searches of yet unidentified *Fermi* gamma-ray sources [15, 14] with suitable spectral parameters have turned out to be the main technique to discover these otherwise elusive eclipsing radio MSPs.

¹ See the list maintained by D. Lorimer & E. Ferrara, available at <http://astro.phys.wvu.edu/GalacticMSPs/GalacticMSPs.txt>

² See the list maintained P. Freire, available at <http://www.naic.edu/~pfreire/GCpsr.html>

3 Changes of state in millisecond pulsars

The multifaceted behaviour of MSPs in tight binaries stems from the balance between the outward pressure exerted by the pulsar wind on the mass lost by the companion star, and the inward gravitational pull applied by the NS gravitational field. Given the typical MSP spin-down power ($L_{sd} \simeq \text{a few} \times 10^{34} \text{ erg s}^{-1}$) and mass transfer rates ($\dot{M} \approx 10^{-3} - 10^{-4} \dot{M}_{Edd}$), this balance enforces within the binary, if the system has a short orbital period ($P_{orb} < 1 \text{ day}$) and a small size ($d \lesssim 10^{11} \text{ cm}$). On one hand, this means that the pulsar wind is terminated by the in-flowing matter in an intrabinary shock. On the other, slight variations in the mass inflow rate may lead to very different outcomes, which in the case of tMSPs occur in quick succession.

In the recycling framework, it was assumed that the accretion and the rotation-powered phases were well distinct. A source was to be found in either one of the states depending on the prevailing of the gravitational or electromagnetic pressure [16, 17]. Fig. 2 shows the radial dependence of these pressures and the three main possible outcomes. The ram pressure of plasma in radial free-fall is [18]:

$$P_{grav} = \frac{(2GM_*)^{1/2} \dot{M}}{4\pi r^{5/2}}, \quad (1)$$

where M_* is the NS mass. In the accretion phase, the high-density plasma fills the light cylinder of the pulsar³ and this was assumed to switch off the rotation-powered pulsar [19]. Some of the closed field lines forming the magnetosphere thread the disc albeit the very high diffusivity of the plasma, and are bent by the differential rotation of the disc material in Keplerian rotation. The disc is truncated at the accretion radius R_{acc} , where the resulting magnetic stress becomes dominant compared to the disc viscous stress. The determination of this radius is crucial to predict the accretion regime onto a magnetised rotator at different accretion rates. It strongly depends on the often unknown micro-physics governing the disc/field interaction and is still a matter of debate (see, e.g., [20, 21]). Under the assumption that the magnetic field lines thread the disc over a large radial extent [22, 23], it turns out that the accretion radius R_{acc} is equal to a fraction ξ of the Alfvén radius R_A , obtained by equating the gravitational energy density (see Eq. 1) with the largest possible magnetic stress:

$$P_{em}(r) = \frac{\mu^2}{8\pi r^6}; \quad r < R_{LC} \quad (2)$$

where $\mu = B_* R_*^3/2$ is the NS magnetic dipole moment, B_* is the field strength at the magnetic poles of the NS, and R_* is the NS radius. This yields:

$$R_{acc} = \xi R_A = \xi \frac{\mu^{4/7}}{\dot{M}^{2/7} (2GM_*)^{1/7}} \simeq 15.4 \xi_{0.5} \mu_{26}^{4/7} \dot{m}_{16}^{-2/7} m_{1.4}^{-1/7} \text{ km}, \quad (3)$$

³ The light cylinder of a pulsar is defined as the cylinder aligned with spin axis, with a radius $R_{LC} = c/2\pi\nu = c/2\pi\nu \simeq 80 \nu_{600} \text{ km}$ (ν_{600} is the spin frequency in units of 600 Hz), where the co-rotating speed of the field lines equals the speed of light. Field lines that would close beyond the light cylinder are forced to open by the causality principle, thus producing the pulsar wind.

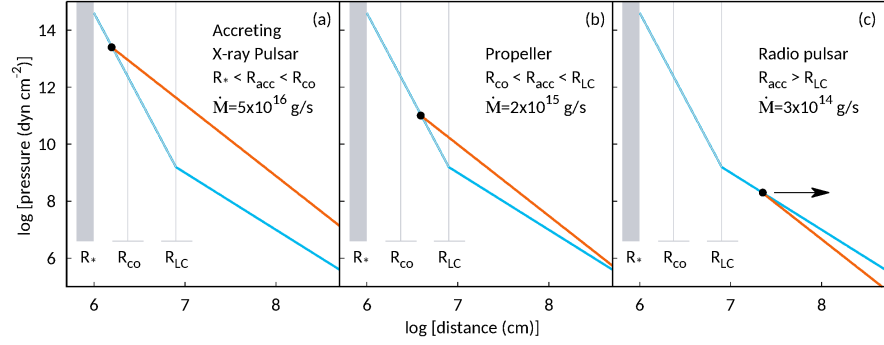


Fig. 2: Dependence of the pressure exerted by the in-flowing plasma (orange lines, Eq. 1) and by the electromagnetic field (cyan lines, Eq. 2 and 5) on the distance from a pulsar with a magnetic dipole moment of 10^{26} G cm³ (corresponding to a field strength at the magnetic poles of 5×10^7 G). Grey vertical lines mark the NS radius (R_*), the co-rotation radius (R_{co}) and the light cylinder radius (R_{LC}) for a pulsar spinning at 600 Hz (corresponding to ≈ 1.67 ms). The three panels represent the possible states depending on the value of the mass accretion rate considered, accreting X-ray pulsar ($R_* < R_{acc} < R_{co}$), propeller ($R_{co} < R_{acc} < R_{LC}$) and rotation-powered radio pulsar ($R_{acc} > R_{LC}$). The arrow indicates evaporation of the intrabinary matter due to the unstable equilibrium in the latter case.

where $\xi_{0.5}$, μ_{26} , \dot{m}_{16} and $m_{1.4}$ are the respective quantities in units of 0.5, 10^{26} G cm³, 10^{16} g s⁻¹ and $1.4 M_\odot$. Alternatively, if the diffusivity of the field lines is low, the magnetic field lines are unable to slip through the disc fast enough, and so they twist and open. The interaction region is smaller and the scaling of the accretion radius are flatter, $R_{acc} \propto \mu^{2/5} \dot{M}^{-1/5}$ [24, 25]. A series of 3D magneto-hydrodynamics simulations of disc accretion onto a magnetised rotating star have indeed given results compatible with such an estimate [26]. However, given the small differences, Eq. 3 with $\xi \approx 0.5$ is still widely used to describe the position of the magnetospheric radius in many astrophysical systems (see, however, [20] for the limitations of the applicability of the magnetospheric radius in Eq. 3).

The subsequent fate of the in-flowing matter depends on whether it has enough angular momentum to overcome the centrifugal barrier set by the rotating pulsar magnetosphere at the disc truncation radius. The co-rotation radius defines where the disc material rotates at the NS spin frequency:

$$R_{co} = \left[\frac{GM_*}{(2\pi\nu)^2} \right]^{1/3} \simeq 23.6 m_{1.4}^{1/3} \nu_{600}^{-2/3} \text{ km.} \quad (4)$$

The in-flowing material either freely accretes onto the NS if $R_{acc} < R_{co}$ (see panel [a] in Fig. 2) or bounces on the barrier set by the rotating magnetosphere in the so-called propeller state if $R_{acc} > R_{co}$ [27] (see panel [b] in Fig. 2).

As the mass accretion rate decreases, the accretion radius expands. When it approaches the co-rotation boundary, no net angular momentum can be transferred to the NS by the in-falling plasma any more. Nevertheless, the field lines which thread the disc beyond the co-rotation radius, and possibly eject matter through the propeller effect, might still exert a spin-down torque [22, 23, 28]. This torque is assumed to limit the secular spin-up of an accreting NS in an LMXB to an equilibrium period of a few milliseconds for a weakly magnetised ($\approx 10^8 - 10^9$ G) NS. Realising that the equilibrium period could be so short was actually the main foundation of the recycling scenario [29].

A further decrease of the mass accretion rate may push the accretion radius beyond the light cylinder, at which point a rotation-powered pulsar is assumed to switch on (see panel (c) in Fig. 2). Outside the light cylinder, a radiative solution describes the pulsar electromagnetic field and its pressure has a much flatter radial dependence than Eq. 2:

$$P_{em}(r) = \frac{L_{sd}}{4\pi r^2 c} \simeq \frac{k\mu^2}{4\pi^2 R_{LC}^4 r^2}; \quad r > R_{LC}. \quad (5)$$

Here $L_{sd} \simeq [\mu^2(2\pi\nu)^4/c^3](1 + \sin^2 \alpha)$ is the pulsar spin-down power [30], and α is the magnetic co-latitude. Since the inflow ram pressure has a steeper dependence on the distance ($P_{grav} \propto r^{-5/2}$, see Eq. 1), the equilibrium for $R_{acc} > R_{LC}$ is expected to be unstable. In this regime the pulsar wind is then expected to expel altogether the intrabinary material from the system and switch-off the mass transfer. In the secular picture, this is expected to take place when the mass transfer rate drops as the donor star detaches from its Roche lobe under the irradiation by the high energy emission of the accreting NS [31, 32, 33].

The idea that binary systems could perform state transitions between accretion and rotation-powered states on a shorter timescale of months/years emerged when many LMXBs hosting NSs were found to undergo transient outbursts (see, e.g., [34]). At the end of an outburst, the pulsar wind was expected to push the accretion disc beyond the light cylinder (i.e., case (c) of Fig. 2). This would allow the turn-on of a rotation-powered radio pulsar during the quiescent period of the transient [35, 36]. The radiation and the wind of relativistic particle so generated would eject the matter from the companion as soon as it entered the pulsar Roche lobe - the so-called radio ejection mechanism [37]. Only an increase of the inward pressure of the transferred matter would allow the X-ray binary to enter in a new accretion outburst. For many years, only circumstantial evidence supported this idea. A few eclipsing MSP binaries were found to expel material transferred from their companions [38] according to a radio ejection scenario [39], but no transition to an accretion stage was observed. On the other hand, accreting MSPs in quiescence gave indirect indications that a radio pulsar switched on, but a detection could not be achieved (see Sec. 5.2). The discovery of tMSPs has eventually filled the gap.

4 Transitional millisecond pulsars

4.1 PSR J1023+0038 – FIRST J102347.6-003841

FIRST J102347.6-003841 was first detected in May 2000 as a variable 1.4 GHz radio source [57]. Double peaked emission lines of the Balmer series, He I and He II in the spectrum and the flickering light curve of its optical counterpart suggested it was a disc accreting binary, possibly a peculiar magnetised white dwarf [57, 58, 59]. In early 2002, the source underwent a dramatic change. An almost sinusoidal smooth modulation at the 4.75 hr orbital period due to heating of the secondary appeared in the optical light curve [60]. Also, emission lines were replaced by a G-type absorption spectrum [40, 59] indicating the disappearance of the disc. Thorstensen et al. [40] first proposed that the binary hosted a quiescent NS, based on the large irradiating luminosity required to explain the optical light curve. The discovery of the 1.67 ms radio pulsar PSR J1023+0038 by the *Robert C. Byrd Green Bank Telescope* in 2007 eventually nailed down this enigmatic object as a redback radio MSP, which had an accretion disc in the previous decade [7]. Archival optical and infrared observations constrained the duration of the 2000/2001 disc episode to $\sim 1.5 - 2$ years [61, 57, 58, 60]. Starting at the end of June 2013, the re-emergence of double-peaked optical emission lines [62], the disappearance of radio pulsations [9], and the brightening of the X-ray, ultraviolet [63] and gamma-ray [9] emissions marked the beginning of a new active phase which is currently ongoing in June 2020. The average X-ray luminosity in the disc state never exceeded $L_X \approx 5 \times 10^{33} \text{ erg s}^{-1}$ (at a parallax distance of 1.37 kpc, [48]), indicating that both the 2000/2001 and the 2013/current accretion episodes have been *sub-luminous* (see Sec. 5.3).

4.2 IGR J18245-2452 – PSR J1824-2452I

The transient X-ray source IGR J18245–2452 in the globular cluster M28 was first detected by *INTEGRAL* in March 2013 during a bright accretion outburst ([64], $L_X \approx 10^{36} \text{ erg s}^{-1}$ at a distance of 5.5 kpc). The *XMM-Newton* detection of 3.9 ms X-ray pulsations identified it as an accreting MSP with a main sequence companion [8]. Cross-referencing with pulsar catalogues, it was realised that the source had been already observed as a radio MSP before (PSR J1824-2452I; [65]), making it the first source both as a rotation-powered and as an AMXP [8]. Radio pulses were again observed after the end of the month-long X-ray outburst in 2013 – two weeks since the last detection of the X-ray pulsar. Serendipitous *Chandra* [8, 66] and *Hubble Space Telescope* observations [49] revealed two more accretion episodes in 2008 and 2009, respectively, which unlike the 2013 outburst, had properties compatible with a *sub-luminous* disc state.

Table 1: Main system properties of tMSPs

	PSR J1023+0038	XSS J1227-4859	IGR J1824-2453	Ref.
P_{orb} (h)	4.75	6.91	11.03	[40, 10, 8]
P_{spin} (ms)	1.69	1.69	3.93	[7, 41, 8]
\dot{P} (10^{-20})	0.539 (RMSP) - 0.713 (LMXB) ^A	1.086	< 0.0013	[42, 43, 41, 8]
$a \sin i$ (lt-s)	0.343	0.668	0.766	[7, 43, 8]
\dot{E}^B (10^{34} erg s ⁻¹)	4.43(4)	$8.9^{+0.2}_{-0.9}$	-	[42, 44]
M_{NS} (M_{\odot})	1.7(2)	-	-	[45]
B_{NS} (10^8 G)	1.9	2.3	0.7-35	[42, 41, 8]
i (deg)	46(2)	46-55	-	[45, 46, 47, 14]
d (kpc)	1.37(4)	$1.4^{+0.7}_{-0.2}$	5.5	[48, 44, 8]
Companion spectral type	G5- >F6	G5- >F5	low main sequence	[40, 46, 49]
Companion mass (M_{\odot})	0.22(3)	0.15-0.36	0.17 ^C	[45, 50, 8]
<i>X-ray properties</i> ^D $F_E \sim E^{-\Gamma}$				
<i>Disc state</i>				
$\Gamma_{X,disc}$	1.62(2)	1.70(2)	1.428(3)	
L_X, ave (10^{33} erg s ⁻¹)	5.2(1)	12(2)	11.2(5)	
L_X, low (10^{33} erg s ⁻¹)	0.87(4)	2.0(4)	2.0(3)	
$L_X, high$ (10^{33} erg s ⁻¹)	7.9(1)	13(3)	13.1(6)	
$L_X, flare$ (10^{33} erg s ⁻¹)	22(6)	70(8)	33	
<i>Rotation-powered state</i>				
$\Gamma_{X,rot}$	1.17(9)	1.2(1)	2.5 assumed	
$L_{X,rot}$ (10^{33} erg s ⁻¹)	0.8(4)	$0.83^{+0.42}_{-0.9}$	< 1	
<i>Gamma-ray properties</i> ^E $F_E \sim E^{-\Gamma}$				
<i>Disc state</i>				
$\Gamma_{\gamma,disc}$	2.41(2)(3)	2.36(6)(9)	-	
$L_{\gamma,disc}$ (10^{33} erg s ⁻¹)	12.5(4)	21.9(7)	-	
<i>Rotation-powered state</i>				
$\Gamma_{\gamma,rot}$	2.31(3)(4)	2.42(3)(15)	-	
$L_{\gamma,rot}$ (10^{33} erg s ⁻¹)	1.1(2)	8.6(8)	-	
<i>Radio properties</i> ^F $S_{\nu} \sim \nu^{\alpha}$				
<i>Disc state</i>				
$\alpha_{r,disc}$	-0.1(2)- >0.2(2)	-0.1(0.1)	-0.2- >0.8	
$L_r, disc, ave$ (10^{27} erg s ⁻¹)	0.97	2.4(8)	123	
$L_r, disc, high$ (10^{27} erg s ⁻¹)	0.63	-	-	
$L_r, disc, low$ (10^{27} erg s ⁻¹)	1.9	-	244	
<i>Rotation-powered state</i>				
$\alpha_{r,rot}$	2.8	-	-	
L_r, rot, ave (10^{27} erg s ⁻¹)	3800	<0.37	-	

^A: Spin down rates in both RMSP and LMXB state determined only for PSR J1023+0038, taking into account also the Shklovskii effect and acceleration in the Galactic potential. ^B: Spin down luminosity assuming the canonical value for the moment of inertia 10^{45} g cm². ^C: Minimum mass. ^D: X-ray luminosity in the 0.3-79 keV range from [52]. ^E: Gamma-ray luminosity in the 0.1-300 GeV using fluxes from [53] and the reported distances at face value. ^F: Radio luminosity at 5 GHz using distances reported at face value and fluxes from [8, 54] for IGR J1824-2452, from [7, 42, 55, 56, 52] for PSR J1023+0038, from [10, 41] for PSR J1227-4853.

^a The NS moment of inertia has been found to range from 1.4×10^{45} g cm² by detailed general relativistic numerical computations using a sample of MSPs with precise NS masses and for several realistic NS EoS models [51].

4.3 XSS J12270-4859 – PSR J1227–4853

XSS J12270-4859 resembles very closely PSR J1023+0038 under many respects (see Table 1). First detected as a hard X-ray source [67], it was tentatively identified as a cataclysmic variable based on the emission lines of its optical spectrum [68] and for large amplitude (~ 1 mag) optical flickering [69]. The spatial coincidence of XSS J12270-4859 with a *Fermi*-LAT source suggested an atypical low-luminosity ($L_X \simeq L_\gamma \simeq \text{few} \times 10^{33} \text{ erg s}^{-1}$) X-ray binary [70, 71]. Its unusual properties were only later assessed to be typical of the *sub-luminous* state of tMSPs ([72, 70, 73, 71, 46], see Sec. 5). The disappearance of the emission lines in the optical spectrum and the 10-fold dimming observed in the radio, optical and X-ray bands (and to a lesser extent in gamma-rays, [53]) demonstrated that XSS J12270-4859 had transitioned from a disc to a radio pulsar state between 2012 November 14 and December 21 [10]. *Giant Metrewave Radio Telescope* observations later detected 1.69 ms radio pulsations eclipsed for a large fraction of the orbit [41]. Since the end of 2012, XSS J12270-4859 still behaves as a rotation-powered redback pulsar.

5 The three states of transitional millisecond pulsars

5.1 The rotation-powered state

In the rotation-powered state, tMSPs behave as redbacks. They are relatively faint objects at all wavelengths, and most of the information we have gathered comes from the study of the closest ones, PSR J1023+0038 and PSR J1227–4853 (see Table 1).

Mass ejection – Irregular eclipses of the radio pulses occur mostly (but not only) when the secondary is at the inferior conjunction of the orbit. They are due to a thin, but dense layer of ionised material which the pulsar wind drives off from the surface of the donor or the inner Lagrangian point, and partly enshrouds the system. The eclipses of PSR J1023+0038 lasted up to $\sim 60\%$ of the orbit when observed at 350 MHz, but were shorter at higher frequencies ($\sim 25\%$ at 1.4 GHz), and nearly absent at ~ 3 GHz [7, 42]. Similarly behaved PSR J1227–4853, showing eclipses for $\sim 40\%$ of the orbit at 607 MHz and $\sim 30\%$ at 1.4 GHz [41, 44]. This can be ascribed to the frequency dependence of the optical depth of the material (e.g., $\propto \nu^{-2}$ for electron scattering, $\propto \nu^{-1}$ for cyclotron absorption [74]) which makes the ionised layer more transparent at high frequencies. The correlated variation of the continuum flux density and the mean pulsed flux density at the eclipse boundary observed from PSR J1227–4853 suggested cyclotron-synchrotron absorption rather than dispersion smearing or scattering [41]. Similar conclusions were also drawn for other spiders [75]. Shorter losses of the signal at random orbital phases and substantial variations of the dispersion measure were also observed. All these properties indicate that the enshrouding ionised plasma extends well beyond the Roche lobe of the donor.

The binary properties – The radio pulsar timing indicated that the orbits of tMSPs and of many spiders are almost circular, with upper limits of the order of a few times 10^{-5} on the eccentricity. This is due to the tidal circularization which occurred during the secular LMXB phase. Irregular changes in the phase of the orbital modulation by a few seconds over timescales of a few months suggested fast apparent orbital period variations [42, 43]. They have been interpreted as a combination of the angular momentum carried by material ejected from the system, and the exchange of angular momentum between the orbit and the companion star due to changes of the mass quadrupole in the latter [76]. Magnetic cycles of the secondary could be the cause for such fluctuations, even though luminosity variations larger than observed would be expected. Recently, a model has been proposed to account for the timing anomalies produced by mass quadrupole deformations in spiders, which is promising to gain insights on the internal structure of their irradiated stars [77].

The optical spectra of PSR J1023+0038 and PSR J1227–4853 displayed absorption features typical of the photosphere of mid G-type stars, primarily metallic and Balmer lines [40, 46, 78, 45]. No spectroscopy has been acquired for the faint counterpart of PSR J1824–2452I, so far. However, photometric observations located it in a position of the colour-magnitude diagram of the globular cluster consistent with a main-sequence star, just 0.5–1 mag below the turn-off point [49]. The lack of an optical and near-infrared polarisation in PSR J1227–4853 suggested that the emission in these bands was only due to the donor photosphere [79]. However, near-ultraviolet photometry of both PSR J1023+0038 and PSR J1227–4853 revealed an excess over the companion emission [47]. This suggests that the emission of the intrabinary shock, which dominates at higher energies (see below), may also extend to the ultraviolet domain.

The optical light curves of these two tMSPs featured an almost sinusoidal modulation at the binary orbital period with an amplitude of $\approx 0.4–0.7$ mag. The emission attains a maximum and becomes bluer when the companion star is at the superior conjunction ([60, 40, 50, 47]; see the right panel of Fig. 3). These signatures are due to the irradiation of the donor by the high-energy emission of the pulsar and were also observed from many spiders [80, 81]. A dramatic change in the spectral type (see Table 1) between the inferior and the superior conjunction confirmed the heating of the donor by the wind of tMSP [46, 45]. Variations in the amplitude of the orbital modulation from epoch to epoch also suggested changes in the heating pattern [50, 45]. In both systems the irradiation persisted also during the disc state [46, 82, 83, 84, 85] with a different heating pattern likely due to disc shadowing of the donor star [45].

Modelling of the multi-colour optical orbital modulation and of the spectroscopic absorption line radial velocity is a technique commonly used to infer the component masses, the Roche lobe filling factor of the companion, and the binary inclination. It is especially powerful when coupled with the NS orbital ephemeris derived from the radio pulsar timing. However, for heated low-mass donors a degeneracy exists between the filling factor and the binary inclination, thus affecting the masses of the components [14]. The two tMSPs in the Galactic field are seen at moderate inclinations [40, 50] (see Table 1). While in PSR J1023+0038 the masses of both

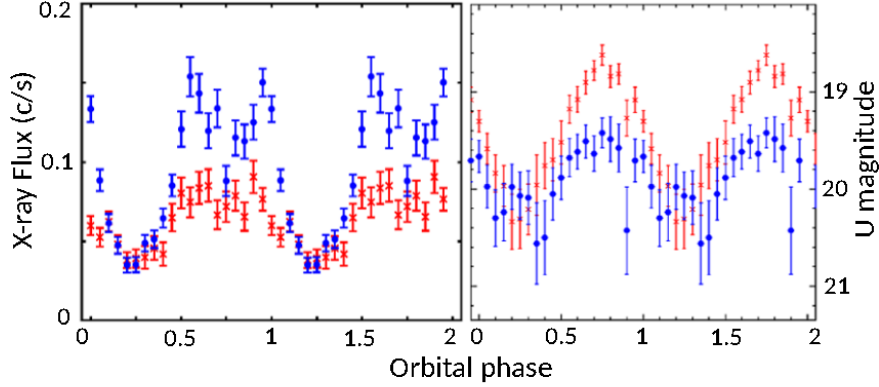


Fig. 3: X-ray (left panel) and optical (right panel) orbital modulation observed from PSR J1227–4853 on 2013, Dec 29 (red points) and 2014, Jun 27 (blue points). Phase 0 corresponds to the passage of the NS at the orbit ascending node. Adapted from [50].

stars could be determined, with an indication of an underfilling donor [78, 45], for PSR J1227–4853 only the donor mass could be constrained.

The X-ray properties and the intrabinary shock – The X-ray luminosity of PSR J1023+0038 [86, 87, 88, 89, 90], PSR J1227–4853 [91, 50, 44] and PSR M28I [92, 8, 66] in the radio-pulsar state ($L_X \approx 1 - 2 \times 10^{32} \text{ erg s}^{-1}$, i.e. $\sim 0.1 - 0.2\%$ of the spin-down power) is at the bright end of the distribution observed in other redbacks ([93], see the bottom panel of Fig. 6). The X-ray spectra of tMSPs were largely non-thermal and described by a power law extending without a break up to $\sim 70 \text{ keV}$ (see Table 1). A soft thermal component possibly emitted by hot spots on the NS surface contributed at most to a few per cent of the $0.1\text{--}10 \text{ keV}$ emission of PSR J1023+0038, while it was not significantly detected in PSR J1227–4853.

A large amplitude ($\gtrsim 25\%$) orbital variability characterised the X-ray emission of tMSPs (see the left panel of Fig. 3), similar to other redbacks [94]. The maximum occurs when the companion is at the superior conjunction, in phase with the radio eclipses and the maximum of the optical emission. Only a slight spectral variability along the orbit has been seen, e.g. a hardening below 3 keV at the inferior conjunction of XSS J12270-4859, and a decrease in the amplitude above 25 keV ([44], Coti Zelati et al., in prep.). This excluded photoelectric absorption to explain the large orbital variability. The observed emission was better modelled with a synchrotron emission from the intrabinary shock created by the interaction of the pulsar wind with the material which issues from the inner Lagrangian point, or directly at the donor surface ([95, 88], see Sec. 6.1). The occultation of the shock by the secondary star when it is at the inferior conjunction of the orbit determines the minimum of the

X-ray emission. The orbital modulation was almost sinusoidal in PSR J1023+0038 with an enhanced emission at eclipse egress [87, 88]. In PSR J1227–4853, instead, the orbital light curve showed a quasi-sinusoidal shape at one epoch but double-peaked when observed 6 months apart. Concurrently, the amplitude of the X-ray modulation varied from 25% to 70%, in anti-correlation with a similar change in the amplitude of the optical modulation ([50], see Fig. 3). Double peaked orbital modulations were also observed from other redbacks such as PSR J2129-0429 [96] and PSR J2339-0533 [97], which also displayed subtle spectral changes along their orbits. The synchrotron emission is expected to be Doppler boosted at the pulsar inferior conjunction and de-boosted at superior conjunction, possibly explaining these features, at least partly ([95, 98], see also Sec.6.1).

X-ray pulsations with a sinusoidal shape and a root-mean-square amplitude of $(11 \pm 2)\%$ were detected below 2.5 keV from PSR J1023+0038 [87]. The pulsed luminosity was a few $\times 10^{-4}$ times the spin-down power, similar to other rotation-powered X-ray MSPs [99]. Sinusoidal profiles are usually ascribed to the heated polar caps on the NS surface [100], although the thermal component observed in the X-ray spectrum was too faint to account for the observed pulse amplitude. A pulsed signal was not detected instead from either PSR J1227–4853 (within an upper limit of 10%, [101]) or PSR M28I (for which high time resolution data lacked [8, 66]).

The gamma-ray emission and particle acceleration – MSPs are energetic enough to convert a few per cent of their spin-down power into emission at GeV energies, and TMSPs made no exception [102]. They were characterised by a luminosity of a few $\times 10^{33} \text{ erg s}^{-1}$ (0.1–100 GeV) and a power law spectrum with photon index $\sim 2.3 - 2.4$ ([103, 104, 105, 53, 106], see Table 1). A marginally significant high energy cut-off at ~ 5 GeV could be detected only in PSR J1227–4853 [53]. Gamma-ray pulsations were reported at a significance of 3.7σ from PSR J1023+0038 [42] and 5σ from PSR J1227–4853 [106]. The gamma-ray (>100 MeV) pulse profile featured a relatively broad peak almost aligned with the main peak of the radio pulse at 1.4 GHz. While an orbital modulation was not detected during the rotation-powered state of PSR J1023+0038, its presence in PSR J1227–4853 is controversial [107, 106].

5.2 Accretion outbursts

So far, IGR J18245–2452 has been the only tMSP that has shown an accretion outburst with a similar peak X-ray luminosity ($L_X \simeq 5 \times 10^{36} \text{ erg s}^{-1}$) and duration (\sim three weeks) than other AMXPs. However, a peculiar and extremely strong variability was seen in two \sim one day-long *XMM-Newton* observations performed a few days apart ([8], see the left panel of Fig. 4). It had an RMS amplitude of more than 90% and its Fourier power density spectrum was described with a power law $P(\nu) \propto \nu^{-\gamma}$ with index $\gamma = 1.2$, extending over six decades in frequency ($10^{-4} - 100$ Hz). Two states could be identified with a flux differing by two orders of magnitude ([54], see the right panels of Fig. 4). In the high-intensity state ($L_X \simeq \text{a few} \times 10^{36} \text{ erg s}^{-1}$, corresponding

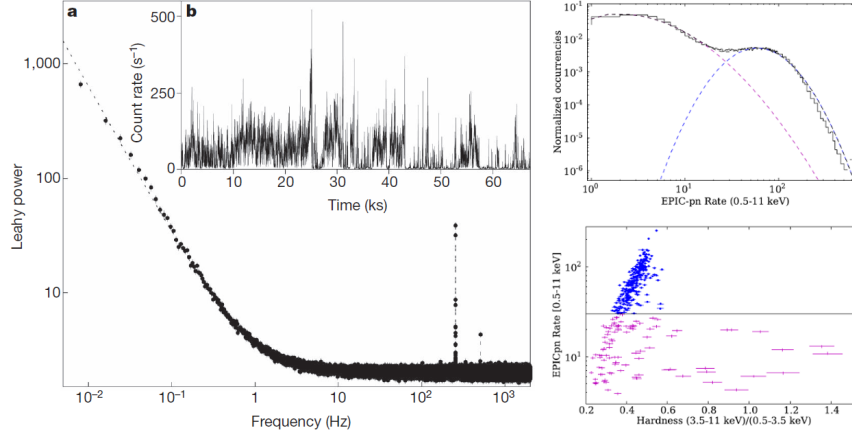


Fig. 4: Left panel: X-ray power density spectrum and light curve (inset) of IGR J18245–2452 observed by *XMM-Newton* during its 2013 outburst. Right panel: Histogram of the X-ray count rates (top panel) and hardness-intensity diagram (bottom panel) showing the two states. Figures are taken from [8, 54].

to a mass accretion rate of $\sim 10^{16} \text{ g s}^{-1} \simeq 10^{-2} \dot{M}_{\text{Edd}}$, a power law $F(E) \propto E^{-\Gamma}$ with $\Gamma \simeq 1.7$ characterised the X-ray energy spectrum. This is typical of AMXPs and is usually interpreted as Compton up-scattering of soft photons coming from the NS surface by hot electrons in the accretion columns. The spectrum became significantly harder, $\Gamma \simeq 0.9$, in the low-intensity state ($L_X \simeq \text{a few} \times 10^{34} \text{ erg s}^{-1}$, corresponding to $\dot{M} \sim 10^{14} \text{ g s}^{-1} = 10^{-4} \dot{M}_{\text{Edd}}$), and an additional partial covering absorption component was required. Together with a strongly variable emission observed at GHz radio frequencies, this suggested the presence of out-flowing material [54]. The spectral hardening characterising the low-intensity state also made the average spectrum of IGR J18245–2452 the hardest of all AMXPs [108]. The X-ray pulse profile showed two sinusoidal peaks per cycle. Pulsations were present at all flux levels up to 60 keV, and the amplitude correlated with flux up to an rms of $\sim 20\%$. In the lower intensity-harder flux state the amplitude was instead lower ($\sim 5\%$) and the shape different. This peculiar behaviour was interpreted in terms of a fast switching between accretion and weak to strong propeller states [109, 54].

Other accreting MSPs in quiescence – IGR J18245–2452 has been the only AMXP detected as a radio pulsar in quiescence, so far. However, many indirect pieces of evidence suggest that a radio pulsar may have switched on also in other AMXPs. When in quiescence, they are relatively faint compared to other soft X-ray transients ($10^{31} - 10^{33} \text{ erg s}^{-1}$; see, e.g., [110]) and show a non-thermal power-law spectrum, possibly originated from an intrabinary shock [111]. On the other hand, a soft thermal component was found to be hardly detectable, giving stringent constraints on the rapidity of the cooling of the NS atmosphere after an accretion outburst [112]. Such a faint X-ray emission could not account for the optical flux of

the irradiated companion, requiring the more intense spin-down power of a rotation-powered pulsar [113, 114, 115]. AMXPs in quiescence spin down at a rate compatible with magneto-rotational torques [116] and their orbit showed a rapid and complex evolution similar to black widow pulsars, possibly due to the ejection of matter from the system [117] and/or angular momentum exchange between the binary and the donor [118]. *Fermi*-LAT data also unveiled a gamma-ray counterpart of the closest ($d = 3.5$ kpc) AMXP known, SAX J1808.4–3658 [119]. The luminosity measured during the ten years between August 2008 and 2018 (in which three outbursts have also occurred) was $L_\gamma = (6 \pm 1) \times 10^{33} \text{ erg s}^{-1}$. This is compatible with the values observed from rotation-powered MSPs, although pulsations could not be detected.

However, despite thorough searches, radio pulses were not detected from AMXPs other than IGR J18245–2452 [120, 121, 122], down to an upper limit of $30 \mu\text{Jy}$ (at 2 GHz) in the case of SAX J1808.4–3658 [118]. An unfavourable inclination (although the radio beams of MSPs are very large), absorption of radio waves at low frequencies (where most of the radio power is emitted) by matter enshrouding the binary, and/or the larger distances of AMXPs (most are located in the Galactic bulge) than transitional systems are possible reasons. Worth noticing is that IGR J18245–2452 was sporadically detected as a faint radio pulsar with a flux density of $10\text{--}20 \mu\text{Jy}$ at 2 GHz, i.e. close to the sensitivity limit, because the M28 cluster where it resides is rich of MSPs, and thus was deeply surveyed in the radio domain [65, 8].

5.3 The sub-luminous disc state

All the three tMSPs showed an enigmatic accretion disc state characterised by an X-ray luminosity of $\sim 10^{33} - 10^{34} \text{ erg s}^{-1}$, fainter than outbursts of AMXPs ($10^{36} - 10^{37} \text{ erg s}^{-1}$) and brighter than rotation-powered MSPs and quiescent AMXPs ($10^{30} - 10^{32} \text{ erg s}^{-1}$). PSR J1023+0038 has a *sub-luminous* disc for 7 years (and counting), with a little change of its properties, if any. XSS J12270-4859 behaved as such between 2003 and 2012, and possibly since earlier times. Shorter episodes were also recorded in PSR J1023+0038 and IGR J18245–2452 (see Sec. 4).

The intensity modes – The *high* (sometimes termed *active*) and the *low* (*passive*) intensity modes observed in the X-ray light curves together with sporadic flares, are perhaps the defining characteristics of tMSPs in the *sub-luminous* state. The top-left panel of Fig. 5 shows an X-ray light curve observed from PSR J1023+0038; the *high* and *low* modes are plotted with blue and red points, respectively, while flares are shown with green symbols. Most of the information about these intensity modes has been obtained from observations of PSR J1023+0038 [63, 82, 89, 83, 123], although they have also been observed from XSS J12270-4859 [72, 70, 71] and IGR J18245–2452 [8, 66] (see [93] for a comparative study). PSR J1023+0038 lies for $\sim 80\%$ of the time in the *high* mode, emitting a roughly constant 0.5–10 keV X-ray luminosity of $\sim 3 \times 10^{33} \text{ erg s}^{-1}$. Unpredictably, sharp transitions to the *low* mode occurs on a timescale of ~ 10 s. The X-ray luminosity observed in the *low* mode is also roughly constant and about one order of magnitude fainter than in the *high* mode, but still a

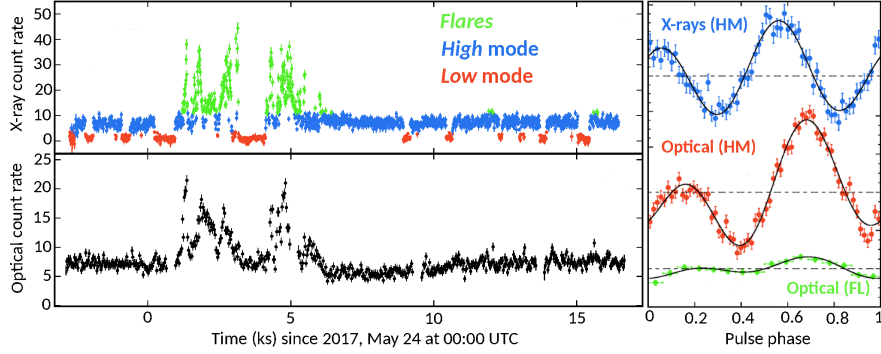


Fig. 5: X-ray (top-left panel) and optical (bottom-left panel) light curves of PSR J1023+0038 in the *sub-luminous* disc state observed simultaneously by *XMM-Newton*. *High mode*, *low mode* and *flares* are plotted in blue, red and green, respectively. The right panel shows the X-ray pulse profile during the *high mode* (blue points) and the optical pulse profiles in the *high* (red points) and *flares* (green points) detected by *SiFAP* at the *INAF Galileo Telescope*. Figure adapted from [56].

few times brighter than the rotation-powered state (see Table 1). The transition from the *low* to *high mode* are characterised by a similar timescale. The duration of these modes ranges from a few tens of seconds to a few hours, although there does not seem to be a characteristic length or recurrence time, nor a correlation between waiting times, duration or luminosity. The luminosity of the *high* and *low modes* have been stable within $\sim 10\%$ in the many observations of PSR J1023+0038 performed so far, without any modulation at the orbital period.

The spectrum of the X-ray emission observed in the *high mode* was described by an absorbed power-law with an index of $\Gamma_X = 1.4 - 1.6$, significantly softer than in the radio pulsar state, $\Gamma \simeq 1.1 - 1.2$ ([93, 83, 124], see Tab 1 and Fig. 6). The power-law extends up to at least ~ 80 keV without evidence for a cut-off [89]. A thermal component with a temperature of ~ 130 eV and contributing to a few per cent of the total flux was also detected at soft X-ray energies in PSR J1023+0038 [83]. Its properties are compatible with the emission coming from the inner rings of a disc truncated ~ 20 km from the pulsar [123]. In the *low mode*, the thermal component disappears and the power-law spectrum becomes slightly softer than in the *high mode* ($\Gamma \simeq 2.0$, [123, 124]).

The X-ray modes observed from XSS J12270-4859 had similar properties. However, the energy spectrum observed in the *low modes* which occurred after a flare was harder than in the *high mode* [70, 71, 93]. The tail of the flaring emission likely contaminated those spectra, indicating that the flaring mechanism is independent of the *high-to-low mode* transitions [125]. An additional partial covering neutral absorber was required to model the spectra of these *low modes*, suggesting a refilling of the matter reservoir close to the NS after a flare [70]. The *high* and *low modes* observed in IGR J18245-2452 had a similar luminosity ratio (~ 7), but lasted significantly

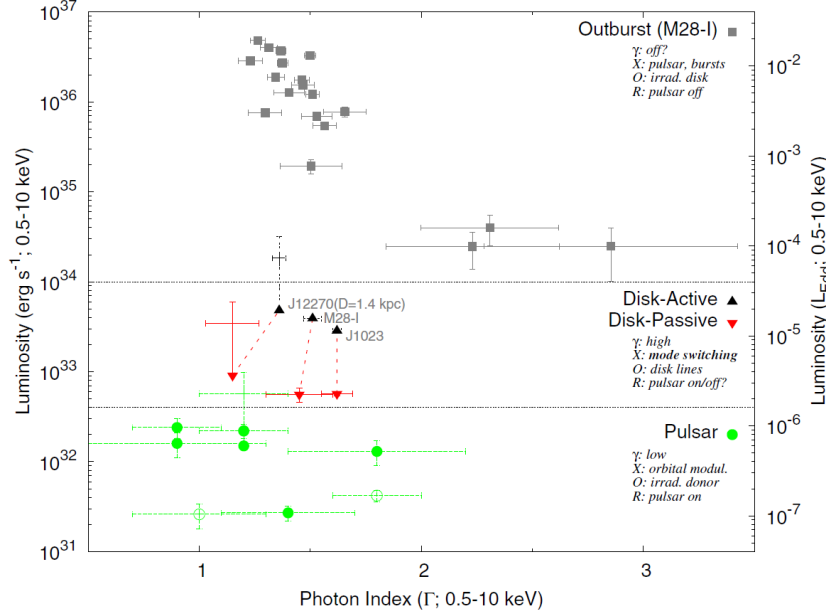


Fig. 6: 0.5–10 keV X-ray luminosity and power-law spectral index of tMSPs in outburst (M28I=IGR J18245–2452) (top panel), in the *high*/active and *low*/passive modes in the *sub-luminous* disc state (middle panel) and of tMSPs and redbacks in the radio pulsar state (bottom panel). Taken from [93].

longer (up to 20 hours) and showed slower transitions ($\sim 500 - 1000$ s), although shorter timescales could not be probed due to the particular observing mode [66, 8].

Flat-bottomed dips were also observed in high-cadence optical observations of PSR J1023+0038 [126, 127]. The ingress/egress times were slightly longer (~ 20 s) than those of X-ray *low* modes, whereas the duration was similar. A bi-modal distribution of the optical flux was also found from a lower cadence *Kepler K-2* monitoring [85]. However, simultaneous optical/X-ray *XMM-Newton* observations have not revealed such dips in B-band data [83, 128], possibly because the optical *low* modes are energy dependent. The lack of simultaneous detection of optical dips and X-ray *low* modes has prevented to establish the relationship between these phenomena, so far. Flares and hints of flat-bottomed dips were also found in near-infrared K_s -band photometric light curves [127]. An enhancement of the near-infrared emission, possibly a flare, was also observed right after an X-ray *low*-to-*high* mode transition [56]. *Low* and *high* modes were much more evident in the ultraviolet; they occurred simultaneously with the X-rays displaying variations by $\sim 25 - 30\%$ in both PSR J1023+0038 [129] and XSS J12270-4859 [70, 71].

The gamma-ray brightening of PSR J1023+0038 when switching from the rotation-powered to the *sub-luminous* disc state, and the gamma-ray dimming of

XSS J12270-4859 in the reverse transition, have been certainly one of the most unexpected features of tMSPs⁴. AMXPs in outburst (and in general LMXBs) have not been detected in gamma-rays, so far⁵. On the other hand, tMSPs in the *sub-luminous* state became a few times brighter than in the rotation-powered state and slightly brighter than in the X-ray band (see Tab. 1). The \sim tenfold gamma-ray brightening observed from PSR J1023+0038 in 2013 took place in a month, or less [9, 53]. The transition of XSS J12270-4859 in the opposite direction was smoother and less pronounced ($L_{\gamma, disc} \sim 2.5 L_{\gamma, rot}$) [106, 53]. The gamma-ray spectra of both tMSPs in the disc state were well described by a power law with index $\Gamma_{\gamma} \approx 2.0$ with marginal evidence of a cutoff between 4 and 10 GeV ([53], see Table 1). A high-energy (> 5 GeV) component was recently claimed to emerge in the spectrum of PSR J1023+0038 at orbital phases corresponding to the pulsar descending node [131], but confirmation with a higher counting statistics is warranted. So far, only upper limits have been set to the emission in the TeV regime [132].

The radio emission – In the *sub-luminous* state of PSR J1023+0038, radio (0.3–5 GHz) pulsations have not been detected in either of the X-ray modes. Upper limits of 0.1–1 mJy were set, i.e. more than an order of magnitude lower than in the radio pulsar state [9, 63, 83]. As the radio emission could be absorbed by the intrabinary material, this does not necessarily imply the complete quenching of the radio pulsar.

A radio continuum emission with a flat or a slightly inverted spectrum was instead seen from both PSR J1023+0038 and XSS J12270-4859 [73, 135]. Similar spectra are ubiquitous among accreting X-ray binaries in the hard state and are interpreted in terms of partially self-absorbed synchrotron emission from out-flowing material [136]. Different correlations hold between the X-ray and the radio luminosity of X-ray binaries hosting black holes and NSs; the latter are generally fainter radio sources at a given X-ray luminosity [133]. In a $L_{radio} - L_X$ diagram (see Fig. 7), tMSPs fall in the radio-bright end of the range expected by propagating the correlation for bright accreting NSs to a lower X-ray luminosity, especially when the peak radio luminosity is considered.

Simultaneous radio and X-ray observations of PSR J1023+0038 unveiled an anti-correlated pattern of variability [55]. When the source switched from the *high* to the *low* X-ray mode, the radio flux suddenly increased and its spectrum became steeper. The decay of the radio emission was instead shallower; it started earlier than the *low-high* mode transition and ended $\sim 30 - 60$ s later. This phenomenology suggested that optically thin emission from expanding plasmoids becomes dominant when the source drops into the *low* mode. Sporadic radio flares up to a few mJy have also been observed in this source [57]. In particular, a radio flare with evolving synchrotron features typical of accretion driven outflows was observed to occur a few minutes after a bright X-ray flare, although other radio flares were observed when the source was in the *high* X-ray mode without any appreciable variability [55].

⁴ The M28 globular cluster to which IGR J18245-2452 belongs, hosts a population of gamma-ray emitting MSPs [130] that made a gamma-ray brightening difficult to detect.

⁵ Note that AMXPs are generally farther ($d \approx 5-8$ kpc) than the two tMSPs in the Galactic field ($d \sim 1.5$ kpc).

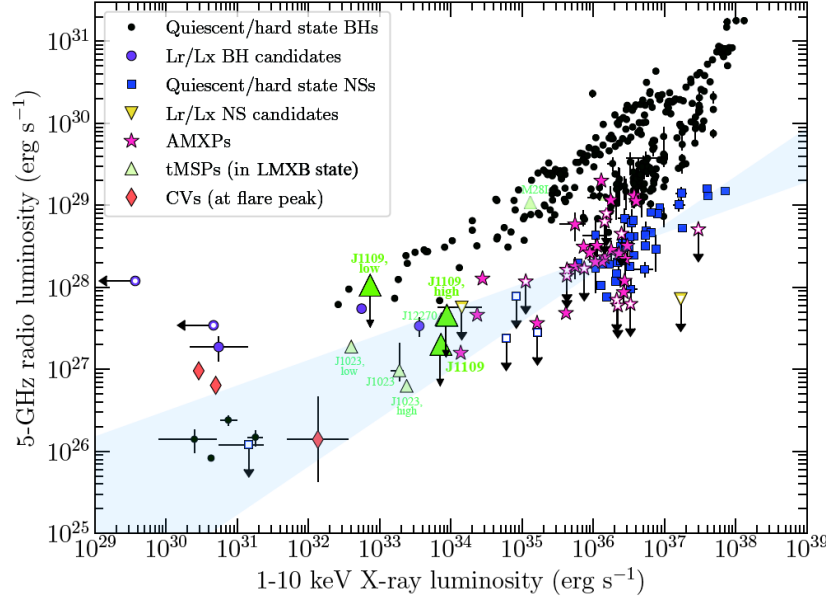


Fig. 7: Radio vs. X-ray luminosity plane for different classes of accreting compact objects. TMSPs in the *sub-luminous* disc state are plotted with green symbols. The cyan shaded area encloses the 3σ confidence interval on the correlation holding for accreting NSs [133]. The figure is taken from [52] and adapted from [134].

The optical/UV emission – The optical brightness of tMSPs in the *sub-luminous* state is $\sim 1 - 2$ magnitudes brighter than in the rotation-powered state, due to the contribution of the newly-formed accretion disc [137, 49, 10]. On the other hand, the donor stars were still found to be heated at a similar level as in the rotation-powered state (see Sec. 5.1). The V and R band emissions in PSR J1023+0038 were found to be linearly polarised at $\sim 1\%$ level possibly due to Thomson scattering within the disc [79, 138].

The optical spectra were dominated by a blue continuum and strong, double-peaked emission lines of H and He produced in an optically thick accretion disc [59, 46, 82, 46, 83]. Modelling of the spectrum of PSR J1023+0038 observed during the 2000-2001 accretion state with a simple disc model gave a temperature in the range $(2 - 34) \times 10^3$ K, and inner and outer radii of $R_{in} \sim 10^9$ cm and $R_{out} \simeq 6 \times 10^9$ cm, respectively [59]. The inner disc radius is larger than the Alfvén radius, indicating that the optical emission originated in the outer disc regions. Similar results were obtained modelling the UV spectrum [139]. In XSS J12270-4859, Doppler tomography showed that the hotter regions producing the He II emission lines were similarly far-out [46].

Flares were observed simultaneously in the X-ray, UV, optical, and near-infrared bands both from PSR J1023+0038 [83, 138] and XSS J12270-4859 [70, 140, 71, 46], suggesting a common underlying process. X-ray flares emitted most of the energy ($L_X \simeq 6 \times L_{opt}$). They lasted from less than a minute to a few hours [71, 83, 43], even though extended episodes lasting up to ten hours have been observed in PSR J1023+0038 [89]. The brightest observed flares attained an X-ray luminosity of $\approx 2 - 7 \times 10^{34} \text{ erg s}^{-1}$ in the 0.3–79 keV band, ([89, 83], see Table 1), slightly exceeding the pulsar spin-down power.

The most prominent optical flares of PSR J1023+0038 had amplitudes of $\sim 0.5 - 1$ mag and lasted up to 14 hours; they traced the brightest flares seen in X-rays with both positive and negative lags of up to ~ 250 s [83]. An 80-days long *Kepler K2* coverage observed optical flares for 15–22% of the time (depending on the flare identification algorithm, [84, 85]), much more frequently than X-ray flares observed at other epochs ($\simeq 2$ per cent, [43]). This showed that the flaring activity is highly unpredictable and cannot be easily parameterised. Multi-band simultaneous observations of a bright event suggested that the flare emission became hotter and more optically thin, like in an accretion disc corona and/or hot fireball ejecta [126]. Similar indications were also found in XSS J12270-4859 [70]. Remarkably, the optical emission lines observed from XSS J12270-4859 [46] and PSR J1023+0038 [138] showed a tendency to disappear during intervals characterised by enhanced flaring emission, compatible with the onset of an outflow. The emergence of an additional polarised component during the flares, possibly due to Thomson scattering from ejected matter, also supported this hypothesis [138]. Flaring variability observed in the near-infrared lagged the optical variability by ~ 10 s, and was tentatively attributed to the reprocessing of the optical emission produced close to the light cylinder by a stream of matter ejected by the system further out [128].

Pulses – X-ray pulsations at the NS spin period were detected only during the *high* mode in both PSR J1023+0038 ([141], see the right panel of Fig. 5) and XSS J12270-4859 [101]. They had an rms amplitude of $\sim 6 - 7$ per cent and were modelled with two sinusoidal harmonic components. Pulsations instead disappeared during the *low* modes and the flares, with upper limits of $\sim 1 - 2\%$. A quasi-coherent timing solution measured over the interval Nov 2013 - Dec 2015 remarkably found that PSR J1023+0038 was spinning down in the disc state at a rate $(32 \pm 2)\%$ larger than in the radio pulsar state [43]⁶.

Quite surprisingly, also the optical emission observed from PSR J1023+0038 turned out to be pulsed with an rms amplitude of $\simeq 1\%$ [142, 56, 143, 144]. This made PSR J1023+0038 the first optical MSP to date. Optical pulsations were detected in the *high* mode and disappeared in the *low* mode with an upper limit of $A < 0.034\%$ ([56]; see the right panel of Fig. 5). Optical and X-ray pulsations had a similar shape with the optical lagging the X-rays by $\sim (200 \pm 70) \mu\text{s}$, an estimate affected by large systematics. The spectral energy distribution of the pulsed emission from the optical to the X-ray band was found to nicely match a power-law relation $F_\nu \propto \nu^{-0.7}$ (see the left panel of Fig. 8). All these properties indicate that the optical and the X-ray

⁶ The fractional change reported here is slightly larger than the value quoted in [43], $(26.8 \pm 0.4)\%$, because it takes into account the Shklovskii effect and acceleration in the Galactic potential [48].

pulsations share a common underlying mechanism [56]. Interestingly, the optical pulses were also detected during flares with an amplitude \sim six times lower than that in the *high* mode [56]. The spin-down rate determined from optical pulsations measured between Jan 2018 and Jan 2020 was $\sim 20\%$ lower than that measured from X-ray pulses at earlier epochs, and closer to the value observed in the radio pulsar state [145]. The difference in the spin-down rate measured from the optical and the X-ray pulsations at different epochs has to be investigated with further long-term coverage in both domains.

5.4 Candidate transitional millisecond pulsars

Stimulated by the discovery of the three tMSPs, searches for new candidates started just after. Searching for a counterpart to a yet unidentified gamma-ray source, with peculiar time variability (such as the *high-low* modes and flares) and spectral properties in the optical (e.g., double peaked emission lines and a blue continuum) and X-ray bands ($L_X(0.3 - 79 \text{ keV}) \simeq (0.5 - 1) \times L_\gamma(0.1 - 300, \text{ GeV})$ and a power law-shaped spectrum with a photon index $\Gamma \sim 1.7$), turned out to be the most efficient way to identify candidate tMSPs in the *sub-luminous* disc state.

RXS J154439.4-112820 was found within the error circle of 3FGL J1544.6-1125. The spectrum of the optical counterpart showed prominent H and He emission lines, consistent with the presence of an accretion disc [146]. The X-ray light curve displayed *high* and *low* modes differing by a factor of ≈ 10 in flux, with transitions occurring on a timescale of $\approx 10 \text{ s}$ [147]. The power-law shaped X-ray spectrum, featuring a photon index $\Gamma \approx 1.7$ and marginal spectral variability, was also similar to those shown by tMSPs in the *sub-luminous* disc state [148]. The long-term optical light curve revealed variability by 0.5 mag and in some occasions enhancements by ≈ 1.0 -1.5 mag [148], reminiscent of the optical flares observed in tMSPs. Optical time-resolved spectroscopy measured a period of 5.8 hr and an inclination of 5 - 8° , implying that the system is seen almost face-on [149]. Adopting a distance prior to the *Gaia* DR2 parallax [150], based on the Galactic model by [151], gave a distance of $1.87^{+1.9}_{-0.72} \text{ kpc}$. The corresponding X-ray and gamma-ray luminosity are $\simeq 3.6 \times 10^{33} \text{ erg s}^{-1}$ and $5.9 \times 10^{33} \text{ erg s}^{-1}$, respectively, very similar to those of tMSPs in the *sub-luminous* disc state.

CXOU J110926.4-650224 (also known as IGR J11098-6457 [152]) is a hard X-ray source located within the error circle of FL8Y J1109.8-6500. The typical modes shown by tMSPs in the *sub-luminous* disc state were easily recognised in its X-ray light curve, and also the energy spectrum was similar to those of the tMSPs [52]. Its variable optical counterpart showed disc emission lines, whereas shallow radio continuum observations could only set an upper limit, still compatible with typical tMSP characteristics. At a distance of $\sim 4 \text{ kpc}$, derived from *Gaia* DR2, the X-ray luminosity is $\simeq 2.2 \times 10^{34} \text{ erg s}^{-1}$, of the same order of the gamma-ray luminosity $\simeq 1.5 \times 10^{34} \text{ erg s}^{-1}$ [52].

Recently, a variable optical and X-ray source has also been found within the error circle of the gamma-ray source **4FGL J0407.7–5702** [153]. The optical spectrum showed double peaked H and He emission lines and a blue continuum indicating the presence of an accretion disc. The X-ray spectrum is also found to be compatible to those observed in tMSPs. The ratio of the X-ray to gamma-ray luminosity was similar to that shown by other sources in the *sub-luminous* disc state, making it a strong candidate tMSP. The comparison of the flux observed in the optical, X-ray and gamma-ray bands with those of other tMSPs in the disc state, and the lack of a significant Gaia parallax, have suggested a distance larger than 5 kpc. This would make it the farthest tMSP known. Although the distribution of the count rates observed in the X-ray band featured two peaks, the phenomenology of the light curve makes an interpretation in terms of the usual *high–low* modes somewhat difficult although the time spent in one or other mode can be different from source to source.

The gamma-ray source **3FGL J0427.9–6704** was recently associated with an accreting eclipsing X-ray binary with an 8.8 hr period and a hard X-ray spectrum extending up to ~ 50 keV [154]. The eclipses were observed both in the X-ray and the gamma-ray light curves, demonstrating the association of the counterpart, and indicating that the high energy emission arose very close to the compact object [154, 155]. The bright and variable emission of the radio counterpart was instead not eclipsed, indicating an origin further out. The X-ray luminosity of this source (5×10^{33} erg s $^{-1}$ at 2.3 kpc) was of the same order of that that observed at gamma-ray energies, similar to tMSPs in the *sub-luminous* state. However, the simultaneous X-ray and optical/ultraviolet light curves did not reveal the typical intensity modes of tMSPs, as the source was found to be flaring for most of the time [156]. Modelling of the optical orbital modulation and of the radial velocity of lines originating from the surface of the $M_2 \sim 0.6 M_\odot$ companion star indicated a relatively massive $\sim 1.8 - 1.9 M_\odot$ NS [154]. However, a recent study based on much higher quality photometric data found a lower, although not highly constrained, mass for the primary ($1.43^{+0.33}_{-0.19} M_\odot$, [155]). Further X-ray observations aimed at detecting the typical modes of tMSPs will constrain the true nature of this candidate.

These characteristics listed above make these sources very strong candidate tMSPs in the *sub-luminous* disc state, although the lack of precise orbital ephemeris has hampered the detection of X-ray pulsations, so far.

The recent release of the 4th *Fermi*-LAT catalogue [157] and its newest 10-yr DR2 version [158]⁷ enhanced the search for MSP binaries associated with an X-ray and optical counterpart. However, discriminating between redbacks and tMSPs in the disc state has been sometimes not immediate. For instance, a few redbacks such as 3FGL J0838.8–2829 [159, 160], PSR J1048+2339 [14] and PSR J1628–3205 [161, 14], the black widow PSR J1311–3430 [162] and the recently discovered long-period (> 1 d) MSP binaries 2FGL J0846.0+2820 [163] and 3FGL J1417.5–4402 [154, 164] occasionally displayed emission lines in their optical spectra. While they may hint to a disc origin, the emission lines could be also ascribed to a magnetically driven wind of the companion. The recently identified source 4FGL J0935.3+0901

⁷ https://fermi.gsfc.nasa.gov/ssc/data/access/lat/10yr_catalog/

has an optical counterpart with double-peaked emission lines, features gamma-ray properties similar to tMSPs, and showed an enhancement by a factor about 8 between Dec. 2010 and Jul. 2013 with significant spectral change [165]. However, its X-ray-to-gamma-ray flux ratio (~ 40) was more typical of spiders in the rotational-powered state rather than of tMSPs in the *sub-luminous* disc state. Simultaneous photometric and spectroscopic observations will be crucial to understand the connection of variable heating and the appearance of emission lines.

Recently, very faint persistent or quasi-persistent X-ray binaries with a luminosity $\sim 10^{33} - 10^{35} \text{ erg s}^{-1}$, have also been proposed to harbour tMSPs in the *sub-luminous* disc state [166]. These sources would switch on as radio pulsars as soon as the X-ray luminosity drops below $\sim 10^{32} \text{ erg s}^{-1}$. However, given the relatively low X-ray luminosity involved, detecting a state transition is only possible for close-by sources or deeply observed fields, such as the Galactic Centre and globular clusters.

Terzan 5 CX10 (CXOG1b J174804.5-244641) is a variable hard X-ray source in the dense globular cluster Terzan 5. A comprehensive study of several *Chandra* observations spanning 13 years found it twice in a bright state with $L_X \sim 2 \times 10^{33} \text{ erg s}^{-1}$ (in 2003 and 2016), and twice in a much fainter state $L_X \sim 10^{32} \text{ erg s}^{-1}$ (between 2009 and 2014) with a harder spectrum than the bright state [134]. This behaviour was reminiscent of the changes of state of tMSPs. A faint optical counterpart with colours compatible with the cluster main sequence was also identified. Follow-up radio continuum observations also revealed a faint ($\sim 20 \mu\text{Jy}$ at 3 GHz) radio source, which placed CX10 close to the position of PSR J1023+0038 in the X-ray/radio luminosity diagram. These properties make it a strong candidate tMSP to be searched in beamed-formed radio observations to reveal the yet to be discovered pulsar.

XMM J174457-2850.3 is a faint X-ray transient in the Galactic centre region. The detection of a 2 hr-long type-I X-ray burst proved that it hosts an accreting NS [167]. This source exhibited a few-weeks long outbursts up to $\sim 10^{36} \text{ erg s}^{-1}$, but for most of the time, it lay in quiescence with a luminosity of $\sim 5 \times 10^{32} \text{ erg s}^{-1}$. Also, it was occasionally found to linger for several months at an intermediate level of $10^{33} - 10^{34} \text{ erg s}^{-1}$ [168]. The X-ray spectrum was described by a $\Gamma \sim 1.4$ power-law, much harder than that generally observed from LMXBs at the same luminosity level. The properties of these three luminosity states resembled those observed in the tMSP IGR J18245-2452 [8]. However, no meaningful search for fast pulsations could be performed either in X-rays due to the low statistic of available data [168], or in the radio band due to the large (6.5 kpc) distance of the source.

Recently, a catalogue of more than 1100 X-ray sources in 38 globular clusters has been compiled to complement the MAVERIC (Milky-way ATCA VLA Exploration of Radio-sources In Clusters) radio survey [169]. Among these, a source in **NGC 6539** was identified as a candidate tMSP based on its X-ray properties, and the presence of a bright radio counterpart with a flat/slightly inverted spectrum. However, this source occupies the same region in the L_X - L_{radio} diagram of black holes and AMXPs (see Fig. 7) and further observations are required to address its true nature.

6 Models and open questions

6.1 The rotation-powered state

The relativistic wind of MSPs in close binaries is terminated by the interaction with the stream of matter issuing from the companion star or the companion star itself. Hence, they offer the opportunity to study the properties of the termination shock so created at much smaller distances than in pulsar wind nebulae. Already in late-80ties, it was also predicted that high-energy photons generated by the particles accelerated at the termination shock would have been able to evaporate the late-type companion star [31, 32, 170]. Models were first applied to the case of the first black widow pulsar discovered, PSR B1957+20 [95]. Given the relatively small size of the binary ($d \simeq 10^{11}$ cm), the magnetic field down-stream the shock is $B \gtrsim 3\sqrt{L_{sd}/cd^2} \approx 30$ G (for a magnetically dominated and isotropic wind emitted by a pulsar with spin-down power $L_{sd} \simeq 10^{34}$ erg s $^{-1}$). Synchrotron emission is thus the main cooling mechanism of the relativistic particles accelerated in the shock, yielding an X-ray output which exceeds the magnetospheric pulsar emission. A recent X-ray study of a large sample of MSPs indeed found that redbacks are brighter than black widows and isolated MSPs [171]. This indicates that a larger fraction of the pulsar wind of redbacks is intercepted at the shock surface compared to black widows.

The luminosity of the shock synchrotron emission depends on the strength of the magnetic field beyond the shock. Assuming that the efficiency of electron acceleration at the shock is similar to that of the Crab pulsar, the relatively bright X-ray luminosity observed from tMSPs required a pulsar wind dominated by the electromagnetic Poynting flux and focused along the equatorial plane of the pulsar (expected to be close to the orbital plane for a spun-up MSP) [88, 91, 44]. The electron population has a power-law energy spectrum with an index p which is related to the power-law index Γ of the X-ray spectrum as $p \sim 2\Gamma - 1$. The X-ray spectrum of both tMSPs [89, 44] and other redbacks observed with *NuSTAR* [172, 96, 97] extended up to at least 70 keV, and was consistent with a power-law with index $\Gamma \sim 1.1 - 1.2$, implying $p \sim 1.3$. Such a value favours a shock-driven magnetic reconnection in a striped pulsar wind (see [173] and reference therein) rather than diffusive shock acceleration. Even though the shock emission has to extend well above the 3–79 keV hard X-ray band covered by *NuSTAR* to be efficient enough in irradiating the secondary star [44], it must be limited below a few MeV not to exceed the pulsar spin-down power. The energy dependence of the orbital modulation marginally seen in two tMSPs (see Sec. 5.1) and PSR J2129-0429 [96] could also hint at a spatial variation of the p -index of the synchrotron emitting electrons.

The prediction that the X-ray emission was modulated at the binary orbital period due to the obscuration by the companion star and to Doppler boosting [95] was indeed confirmed in several MSP binaries [174, 94]. The phasing of the X-ray orbital modulation observed in tMSPs is similar to that observed in other redbacks; the X-ray flux attains a maximum when the pulsar is at the inferior conjunction of the orbit, in phase with the optical orbital variability [94]. On the contrary, the

X-ray modulation of black widows displays a minimum when the pulsar is at the inferior conjunction of the orbit. To explain this, a different orientation of the shock in redbacks and black widows has been proposed by two groups [81, 175, 176], who have developed semi-empirical models to explain the radio, X-ray and optical behaviour. They argued that the shock which surrounds redbacks is oriented towards the pulsar due to the large companion wind momentum $\beta_w = \dot{M}_2 v_w c / \dot{E}$ (where v_w is the relative wind velocity and \dot{M}_2 is the mass loss rate), while it surrounds the companion in black widows. The wind momentum ratio also sets the shock opening angle, which together with the binary inclination in turn determines the shape of the X-ray orbital light curve, single or double-peaked; the width of the peaks depends instead on the boost parameter [98, 175]. Most redbacks showed a rather stable X-ray double-peaked modulation, while the tMSP PSR J1227-4853 displayed variations from single to double and again single-peaked shape over several months, indicating changes in the shock parameters [50, 44]. It was also noticed that systems prone to make or just after a transition, may indeed display variability in the shape of X-ray orbital modulation [175].

The stability of the shock over years is still an unresolved issue since a quasi-radial infall terminated outside the pulsar light cylinder is unstable on dynamical timescales ([37]; see Sec. 3). It was suggested that either a highly magnetised ($B \sim$ several kG) donor star with and low mass-loss rate ($\lesssim 10^{15} \text{ g s}^{-1}$, [42]), or a secondary star with a large mass loss rate but with an ADAF-like or heating-dominated flow, could bend the shock towards the pulsar helping make it stable [176]. This flow should be unmodulated and detectable at soft X-rays down to UV wavelengths and could explain the observed UV excess in PSR J1227-4538.

The companion star heating pattern inferred from high-quality optical photometric light curves of both redbacks and black widows did not match what expected from direct irradiation by the pulsar only, requiring also the illumination by the intrabinary shock [81]. An additional source of heating could arise if a fraction of the wind particles threads the companion field lines and is ducted to its surface; this would require a very active magnetic star displaying star-spots or flares [177, 176]. This possibility was claimed to explain the optical light curve of the strongly irradiated companion of the redback PSR J2215+5135 [177]. Asymmetries in the optical orbital modulation were also observed in the tMSP PSR J1227-4853, although no indication of a magnetically active star was found [50].

6.2 The accretion-disc state

Transitional systems have shown a marked preference for the *sub-luminous* disc state than the bright X-ray outbursts typically seen from AMXPs. This made them more elusive to discover, and hard to reconcile with the typical classification scheme of X-ray transients. The main features of the *sub-luminous* state to explain are:

- its duration (more than ~ 10 years) and faintness (the accretion rate estimated from the X-ray luminosity is 5×10^{-5} times the Eddington rate);

- the *high* and *low* intensity modes with fast (~ 10 s) transitions seen in X-rays and UV, as well as in the optical and near-infrared, although with a still uncertain relationship with the other bands;
- the X-ray and optical pulsations detected in the *high* mode;
- the spin down of the NS, at a rate somewhat higher than in the rotation powered state;
- a radio brightening occurring simultaneously to the X-ray *low* modes and attaining a luminosity comparable to black hole binaries in the hard state at the same X-ray luminosity;
- an increased gamma-ray emission ($L_\gamma \gtrsim L_X$) compared to the rotation-powered state;
- flares seen in the X-rays, UV, optical and near-infrared bands, with duration ranging from several minutes to hours.

Determining whether the multi-wavelength emission observed in the *sub-luminous* disc state is accretion or rotation-powered is the major challenge. This is not surprising since the accretion luminosity estimated from the X-ray flux is comparable to the pulsar spin-down power ($\approx \text{few} \times 10^{34} \text{ erg s}^{-1}$), and both processes should be important. Most of the models proposed so far relied on the standard assumption that the source emission could be either accretion or rotation-powered. In the accretion-powered case the intrusion of high-density accreting plasma into the magnetosphere would easily suppress the acceleration of particles in the magnetosphere and the resulting emission [16, 19, 17]. On the other hand, the switch on of a rotation-powered radio pulsar would develop a radiation pressure which is able to eject the material lost by the companion [37]. However, the complications in applying one or the other assumption to the *sub-luminous* state of tMSPs have forced to consider models in which both rotation and accretion-powered mechanisms conspire to yield the puzzling emission properties listed above.

Enshrouded radio pulsar models - The unexpectedly bright gamma-ray emission of tMSPs first led Takata et al. [105, 90] and Coti Zelati et al. [82] to argue that a radio pulsar was hiding behind the enshrouding intrabinary matter [170]. They assumed that the pulsar wind truncated the disc far from the pulsar ($d \approx 10^9 - 10^{10} \text{ cm}$). The electrons accelerated in the shock would up-scatter the disc UV photons to yield the observed gamma-rays. These electrons would also interact with the field permeating the shock to emit synchrotron X-ray photons.

These models were proposed before the optical and X-ray pulsations had been discovered. Although the magnetosphere of a rotation-powered pulsar could produce these pulsations, the efficiency in converting the spin-down power into optical and X-ray pulsed emission (a $\text{few} \times 10^{-4}$ and 6×10^{-3} , respectively for PSR J1023+0038) should be higher than in young rotation-powered optical (see Fig. 3 in [142]) and X-ray pulsars (see [171]). Also, the X-ray efficiency should have increased by ~ 25 times after the formation of the disc. This would be hard to understand since the magnetospheric processes of the pulsar should not be affected by a disc truncated much further out. Besides, the synchro-curvature models which provided a successful modelling of the X-ray/gamma-ray emission of other MSPs [178, 179], failed to do so for tMSPs in the disc state.

Accretion/propeller models - The detection of X-ray pulsations with similar properties of the pulses of AMXPs suggested that accretion onto the NS magnetic poles was taking place also in tMSPs [141, 101]. However, this would make tMSPs the faintest accreting X-ray pulsars known. This is a critical issue since the mass accretion rate deduced from the observed X-ray luminosity ($\dot{M} \simeq 5 \times 10^{13} \text{ g s}^{-1} = 5 \times 10^{-5} \dot{M}_{Edd}$) would place the accretion radius well beyond the co-rotation radius (e.g. $R_{acc} \sim 75 \text{ km}$ and $R_{co} \simeq 25 \text{ km}$ in PSR J1023+0038, see eq.s 3 and 4). A centrifugal barrier would be expected to inhibit completely the accretion inflow [27]. Magneto-hydrodynamic simulations [180] have shown that if the magnetosphere rotates only slightly faster than the disc matter ($R_{acc} \gtrsim R_{co}$), the propeller is *weak*; part of the in-flowing mass manages to accrete and produce X-ray pulsations, the rest is bounced back to the disc in a non-collimated wind. Therefore, various attempts have been made to keep the accretion radius close to co-rotation at such a low \dot{M} , such as considering a high NS magnetic dipole inclination [21].

Papitto et al. [181, 182] argued instead that the mass accretion rate in the disc was higher than that deduced from the X-ray luminosity, so maintaining the accretion radius obtained with Eq. 3 close to the co-rotation surface. The propeller effect would eject most (>90%) of the disc mass with a low emission efficiency, and only a tiny fraction would make its way to the NS surface. Electrons would be accelerated at the magnetised ($B \sim 10^5 - 10^6 \text{ G}$) turbulent disc/magnetosphere boundary and emit X-ray synchrotron photons. The Compton up-scattering of these photons up to a few GeVs in a few km-wide region would account for the gamma-ray emission.

Following D’Angelo et al. [25, 183, 184], it was alternatively proposed that the disc of tMSPs could be trapped in a low \dot{M} state, so avoiding the onset of a propeller [43]. The in-flowing matter would pile up at the co-rotation boundary rather than being ejected from the system, and the disc truncation radius would be locked close to the co-rotation boundary without any strong dependence on \dot{M} (see also [185] who obtained a similar result in the propeller framework).

The transitions between the *high* and *low* intensity modes could be due to a switching between an accretion/propeller and a rotation-powered state, respectively [66, 123]. In the *low* mode, the pulsar wind would be terminated in a shock beyond the light cylinder, which would hide the radio pulses [82] and produce the power-law shaped X-ray spectrum. In the *high* mode, the disc would get close to the co-rotation radius, with most of the emission produced at the boundary between the disc and the propelling magnetosphere [123]. The penetration of the disc within the light cylinder would force some magnetic field lines to open [186], explaining the enhanced spin-down observed in the disc state compared to the radio pulsar state [43, 187, 145].

Bhattacharyya [188] has recently included such an additional spin-down component in the torque budget. The fraction of magnetic field lines opened by the disc intrusion inside the light cylinder was estimated from the observed increase of the γ -ray emission. The underlying non-standard assumption was that the magnetospheric processes invoked to explain the high energy emission in the rotation-powered state kept working in the disc state, even if the in-falling plasma was accreting onto the NS surface so driving the X-ray pulsations. Since the accretion torques are negligible compared to the pulsar spin-down torques, the overall budget could be ensured only

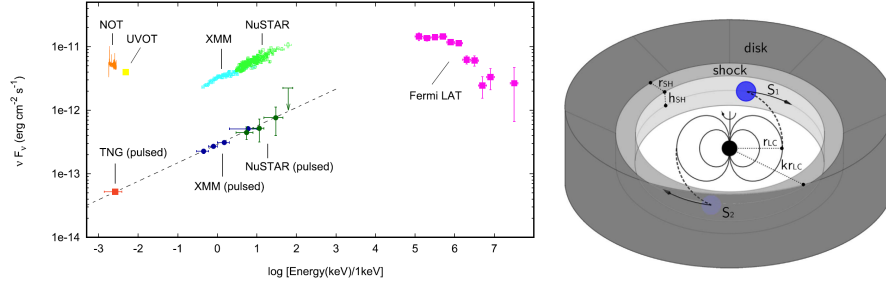


Fig. 8: Spectral energy distribution of PSR J1023+0038 in the *sub-luminous* disc state (left panel). Sketch of the mini pulsar-wind nebula configuration, taken from [56] (right panel).

by the inclusion of an additional spin-down torque. Such a component could be granted by the continuous gravitational radiation related to a permanent ellipticity of the NS yielding a quadrupole moment of $Q \simeq 1 - 2 \times 10^{36} \text{ g cm}^2$.

The increased spin-down due to the emission of gravitational waves had been first considered by Haskell & Patruno [189]. They assumed that asymmetries in pycnonuclear reactions or an unstable r-mode developing in the accretion state only could yield a NS mass quadrupole moment of $> 4.4 \times 10^{35} \text{ g cm}^2$, strong enough to account for the observed increase of the spin-down. Deriving fully coherent X-ray and optical pulse timing solutions in the disc state, and a radio pulse timing solution at the onset of the next radio MSP phase will test this intriguing possibility, which predicts a gravitational wave amplitude in the range of the next generation interferometers such as the Einstein telescope.

Alternatively, Ertan [185] argued that the sub-luminous disc state and the radio pulsar state represented weak and strong propeller states (although there is no strong evidence of the presence of a disc extending close to the NS when radio pulses are observed); a decrease of the accretion radius in the weak propeller state would account for the increased propeller torque.

A mini pulsar-wind nebula – The detection of relatively bright optical pulsations from a tMSP in the disc state was hard to fit in the accretion framework [142, 56]. The cyclotron self-absorbed optical emission produced in the accretion columns is expected to be much fainter than the values observed. A beaming of the emission by a factor of ~ 50 would be required to match the observations, but it seems unlikely given the sinusoidal shape of the pulses. The simultaneous appearance and disappearance of optical and X-ray pulsations, the similar shape and the possibility of describing the optical/X-ray pulsed spectral energy distribution with a single power-law, strongly suggested that they are produced by a common underlying process. As a consequence also the accretion interpretation of the X-ray pulses had to be questioned. Papitto et al. [56] and Veledina et al. [190] proposed that the disc was truncated just beyond the light cylinder also in the *high* mode and that both optical and X-ray pulsations originated at the pulsar wind termination shock. In the so-called

striped wind models (see, e.g., [191]), two current sheets carry the electromagnetic power of the pulsar wind outside the light cylinder. These would produce two rotating spots in the inner face of the wind/disc boundary in which particles are accelerated and quickly radiate optical and X-ray synchrotron photons, by interacting with the relatively strong field ($\approx \text{few} \times 10^5$ G) that permeates the shock. An observer would see these spots from a different angle at each rotational phase, so explaining the detection of coherent optical and X-ray pulsations (see the right panel of Fig. 8). Indeed, the narrow emission and absorption lines observed at a few keV supported the presence of a hot and dense turbulent medium close to the light cylinder [124]. In the *low* intensity mode, the termination shock would be pushed outward and the pulsations would be smeared because the synchrotron emission time scale and the light travel time between different regions of the shock become longer [56]. In the *high* mode, the shock would instead approach the light cylinder, justifying the need of an additional absorbing component covering 30% of the emitting source to explain the change of the X-ray emission spectrum compared to the *low* mode [192, 125]. Alternatively, the *low* mode could be ascribed to the penetration of the disc plasma inside the light cylinder which would curb the termination shock emission [190]. Axisymmetric general-relativistic MHD simulations demonstrated that the pulsar electromagnetic wind can keep the plasma inflow beyond the light cylinder, creating a termination shock and inhibiting mass accretion [193]. Placing the termination shock close to the light cylinder would also help solve the stability issue of the equilibrium between the pulsar wind and the matter inflow beyond the light cylinder [194]. In this framework, episodes of magnetic reconnection at the termination shock, in the disc or from the donor star could also explain the observed flares [192].

Outflows – The bright continuous radio emission [54, 135, 55] and the obscuration of the disc emission lines at certain orbital phases [46] suggested that tMSPs launch outflows of plasma. The radio emission observed in the *high* mode is compatible with self-absorbed synchrotron emission from a compact jet, whose spectral break would be beyond the near-infrared band given the low accretion luminosity [128]. Less collimated outflows could also be launched by the propelling magnetosphere [181, 182] or by the pulsar wind [56].

On the other hand, a compact jet could hardly explain the radio brightening observed in the *low* X-ray intensity mode, since a correlation between the radio and X-ray luminosity would be expected. The sudden radio brightening at the onset of an X-ray *low* mode indicated that the emission had to come from the vicinity of the NS. The launching of optically thin plasmoids by episodes of magnetic reconnection due to the complex field/disc interactions in the pulsar-wind framework [193] was considered the most likely explanation [55, 56, 190]. The reconnection of magnetic field lines threading the disc, or of the donor star, could also explain the flares observed at all wavelengths [192].

The variability – Simulations of the complex interaction between the pulsar electromagnetic field and the disc plasma in a regime in which they have comparable energy densities [180, 193] helped understand the qualitative behaviour of tMSPs. However, they are limited to timescales of less than a second. The long-term changes

of state, the *high-low* mode transitions and in general the flicker noise variability lasting up to a few hours, were clearly out of reach.

The swings between accretion and rotation-powered activity over a few years are generally attributed to changes in the ram pressure exerted by the matter captured by the gravitational field of the NS. However, it remains unclear what ultimately causes the \dot{M} to vary. A viscous disc instability is usually invoked to explain the transient behaviour of dwarf novae and X-ray binaries [195]. TMSPs challenged this interpretation since two very different accretion disc states were realised, a bright and a *sub-luminous* one. An advection dominated accretion flow may characterise the fainter state, and a more typical geometrically thin/optically thick disc the former. However, it is puzzling that IGR J18245–2452 (and possibly XMM J174457–2850.3) was able to show both states just a few years apart. Also, it is not yet determined whether a disc-like flow manages to survive the pulsar wind pressure in the rotation-powered state (see Sec. 6.1). Variations in the mass-loss rate from the donor are unlikely driven by changes of its radius since the timescales involved are much longer even when high energy irradiation of the donor is considered. The magnetic activity of the secondary excited by its fast orbital-locked rotation is instead an intriguing possibility to drive surges of the mass transfer rate needed to squeeze the pulsar wind and start the formation of an accretion disc.

The driver of the recurring *high-low* mode transitions so frequently observed in the *sub-luminous* state, despite a chaotic and unstable disc/wind interaction, is also yet to determine. A flicker noise power-law extending to very low frequencies (10^{-3} – 10^{-4} Hz) characterised the X-ray power density spectra of both the bright outburst of IGR J18245–2452 and the *sub-luminous* states. Similar spectra have been sometimes observed from a few black hole binaries in the soft state, while the noise power density of AMXPs becomes flat below 0.1–1 Hz [196]. The fluctuations of the mass inflow rate in the outer disc, where the viscous time-scales are long, are usually invoked to explain such spectra [197]; these fluctuations must be able to propagate to the inner disc regions to produce the observed X-ray variability. In this framework, the *high-low* mode transitions occurring in tMSPs in the *sub-luminous* state (but also the two intensity states observed from IGR J18245–2452 in outburst, [54]) could reflect how the \dot{M} variations introduced in the outer disc eventually force the system into two well-defined luminosity states, related to the different regimes (accretion, propeller, radio pulsar) introduced earlier.

7 Conclusions

A decade of observations of tMSPs demonstrated that variations in the mass inflow rate lead to very different states in quick succession. This unique property has allowed us to study the complex interaction between the in-flowing plasma and the pulsar electromagnetic field in different regimes.

Multi-wavelength and high-temporal resolution simultaneous observations of tMSPs have been crucial to glimpse the physical processes lying behind the *sub-luminous*

disc state. Much has to be done yet, especially to understand the nature of the modes and the flares that characterise this state. For instance, establishing whether the X-ray and optical pulsations originate just outside the light cylinder, implying that the pulsar wind is terminated a few km away, would have important consequences to confirm the striped wind configuration and measure how it interacts with the surrounding matter. On one hand, searches for more optical MSPs in either accretion or rotation-powered systems will assess the nature of optical pulsations. On the other, MHD simulations will help investigate the properties of the disc/wind intrabinary shock. In this regard, studies of tMSPs could play an important role as a benchmark for the theories that assume that a millisecond magnetar form after a double NS merger and powers a short gamma-ray burst.

Searches for new systems associated with gamma-ray sources and displaying a peculiar X-ray and optical behaviour are intensively ongoing. Together with the monitoring of redbacks and AMXPs, this will likely increase the number of confirmed tMSPs. This will be crucial to assess whether all the MSPs in tight binaries are potentially transitional, or other properties (e.g. magnetic activity of the secondary, magnetic inclination) are required to yield the state transitions. Enlarging the sample has important consequences in the understanding of the population of short orbital period MSP binaries, rather than restricting to the case by case, as done so far.

8 Acknowledgements

We acknowledge financial support from the Italian Space Agency (ASI) and National Institute for Astrophysics (INAF) under agreements ASI-INAF I/037/12/0 and ASI-INAF n.2017-14-H.0 and from INAF "Main streams", Presidential Decree 43/2018 and "SKA/CTA projects", Presidential Decree N. 70/2016. We acknowledge fruitful collaboration with F. Ambrosino, E. Bozzo, L. Burderi, M. Burgay, S. Campana, F. Coti Zelati, P. D'Avanzo, T. Di Salvo, C. Ferrigno, A. Ghedina, A. Miraval Zanon, F. Meddi, E. Poretti, A. Possenti, N. Rea, A. Sanna, L. Stella, D. F. Torres, and many more with whom we have faced the challenge of tMSPs in the last decade.

References

1. M.A. Alpar, A.F. Cheng, M.A. Ruderman, J. Shaham, *Nature*, **300**(5894), 728 (1982). DOI 10.1038/300728a0
2. V. Radhakrishnan, G. Srinivasan, *Current Science* **51**, 1096 (1982)
3. A.C. Fabian, J.E. Pringle, F. Verbunt, R.A. Wade, *Nature*, **301**(5897), 222 (1983). DOI 10.1038/301222a0
4. D. Bhattacharya, E.P.J. van den Heuvel, *PhR*, **203**(1-2), 1 (1991). DOI 10.1016/0370-1573(91)90064-S
5. A.G. Lyne, A. Brinklow, J. Middleditch, et al., *Nature*, **328**(6129), 399 (1987). DOI 10.1038/328399a0
6. R. Wijnands, M. van der Klis, *Nature*, **394**(6691), 344 (1998). DOI 10.1038/28557

7. A.M. Archibald, I.H. Stairs, S.M. Ransom, et al., *Science* **324**(5933), 1411 (2009). DOI 10.1126/science.1172740
8. A. Papitto, C. Ferrigno, E. Bozzo, et al., *Nature*, **501**(7468), 517 (2013). DOI 10.1038/nature12470
9. B.W. Stappers, A.M. Archibald, J.W.T. Hessels, et al., *ApJ*, **790**(1), 39 (2014). DOI 10.1088/0004-637X/790/1/39
10. C.G. Bassa, A. Patruno, J.W.T. Hessels, et al., *MNRAS*, **441**(2), 1825 (2014). DOI 10.1093/mnras/stu708
11. A. Patruno, A.L. Watts, arXiv e-prints arXiv:1206.2727 (2012)
12. S. Campana, T. Di Salvo, *Accreting Pulsars: Mixing-up Accretion Phases in Transitional Systems* (2018), vol. 457, p. 149. DOI 10.1007/978-3-319-97616-7_4
13. M.S.E. Roberts, in *Neutron Stars and Pulsars: Challenges and Opportunities after 80 years, IAU Symposium*, vol. 291, ed. by J. van Leeuwen (2013), *IAU Symposium*, vol. 291, pp. 127–132. DOI 10.1017/S174392131202337X
14. J. Strader, S. Swihart, L. Chomiuk, et al., *ApJ*, **872**(1), 42 (2019). DOI 10.3847/1538-4357/aafbaa
15. D. Salvetti, R.P. Mignani, A. De Luca, et al., *MNRAS*, **470**(1), 466 (2017). DOI 10.1093/mnras/stx1247
16. V.F. Shvartsman, *SvA*, **14**, 527 (1970)
17. V.M. Lipunov, *ApSS*, **132**(1), 1 (1987). DOI 10.1007/BF00637779
18. K. Davidson, J.P. Ostriker, *ApJ*, **179**, 585 (1973). DOI 10.1086/151897
19. V.F. Shvartsman, *SvA*, **15**, 342 (1971)
20. E. Bozzo, L. Stella, M. Vietri, P. Ghosh, *A&A*, **493**(3), 809 (2009). DOI 10.1051/0004-6361:200810658
21. E. Bozzo, S. Ascenzi, L. Ducci, et al., *A&A*, **617**, A126 (2018). DOI 10.1051/0004-6361/201732004
22. P. Ghosh, F.K. Lamb, *ApJ*, **234**, 296 (1979). DOI 10.1086/157498
23. Y.M. Wang, *ApJ*, **449**, L153 (1995). DOI 10.1086/309649
24. H.C. Spruit, R.E. Taam, *ApJ*, **402**, 593 (1993). DOI 10.1086/172162
25. C.R. D’Angelo, H.C. Spruit, *MNRAS*, **406**(2), 1208 (2010). DOI 10.1111/j.1365-2966.2010.16749.x
26. A.K. Kulkarni, M.M. Romanova, *MNRAS*, **433**(4), 3048 (2013). DOI 10.1093/mnras/stt945
27. A.F. Illarionov, R.A. Sunyaev, *A&A*, **39**, 185 (1975)
28. S.A. Rappaport, J.M. Fregeau, H. Spruit, *ApJ*, **606**(1), 436 (2004). DOI 10.1086/382863
29. G. Srinivasan, E.P.J. van den Heuvel, *A&A*, **108**, 143 (1982)
30. A. Spitkovsky, *ApJ*, **648**(1), L51 (2006). DOI 10.1086/507518
31. W. Kluzniak, M. Ruderman, J. Shaham, M. Tavani, *Nature*, **334**(6179), 225 (1988). DOI 10.1038/334225a0
32. M. Ruderman, J. Shaham, M. Tavani, *ApJ*, **336**, 507 (1989). DOI 10.1086/167029
33. M. Ruderman, J. Shaham, M. Tavani, D. Eichler, *ApJ*, **343**, 292 (1989). DOI 10.1086/167704
34. N.E. White, *A&AR*, **1**(1), 85 (1989). DOI 10.1007/BF00872485
35. L. Stella, S. Campana, M. Colpi, et al., *ApJ*, **423**, L47 (1994). DOI 10.1086/187232
36. S. Campana, M. Colpi, S. Mereghetti, et al., *A&AR*, **8**(4), 279 (1998). DOI 10.1007/s001590050012
37. L. Burderi, A. Possenti, F. D’Antona, et al., *ApJ*, **560**(1), L71 (2001). DOI 10.1086/324220
38. N. D’Amico, A. Possenti, R.N. Manchester, et al., *ApJ*, **561**(1), L89 (2001). DOI 10.1086/324562
39. L. Burderi, F. D’Antona, M. Burgay, *ApJ*, **574**(1), 325 (2002). DOI 10.1086/340891
40. J.R. Thorstensen, E. Armstrong, *AJ*, **130**(2), 759 (2005). DOI 10.1086/431326
41. J. Roy, P.S. Ray, B. Bhattacharyya, et al., *ApJ*, **800**(1), L12 (2015). DOI 10.1088/2041-8205/800/1/L12
42. A.M. Archibald, V.M. Kaspi, J.W.T. Hessels, et al., arXiv e-prints arXiv:1311.5161 (2013)
43. A. Jaodand, A.M. Archibald, J.W.T. Hessels, et al., *ApJ*, **830**(2), 122 (2016). DOI 10.3847/0004-637X/830/2/122

44. D. de Martino, A. Papitto, M. Burgay, et al., *MNRAS*, **492**(4), 5607 (2020). DOI 10.1093/mnras/staa164
45. T. Shahbaz, M. Linares, P. Rodríguez-Gil, J. Casares, *MNRAS*, **488**(1), 198 (2019). DOI 10.1093/mnras/stz1652
46. D. de Martino, J. Casares, E. Mason, et al., *MNRAS*, **444**(4), 3004 (2014). DOI 10.1093/mnras/stu1640
47. L.E. Rivera Sandoval, J.V. Hernández Santisteban, N. Degenaar, et al., *MNRAS*, **476**(1), 1086 (2018). DOI 10.1093/mnras/sty291
48. A.T. Deller, A.M. Archibald, W.F. Brisken, et al., *ApJ*, **756**(2), L25 (2012). DOI 10.1088/2041-8205/756/2/L25
49. C. Pallanca, E. Dalessandro, F.R. Ferraro, et al., *ApJ*, **773**(2), 122 (2013). DOI 10.1088/0004-637X/773/2/122
50. D. de Martino, A. Papitto, T. Belloni, et al., *MNRAS*, **454**(2), 2190 (2015). DOI 10.1093/mnras/stv2109
51. S. Bhattacharyya, I. Bombaci, D. Bandyopadhyay, et al., *NewA*, **54**, 61 (2017). DOI 10.1016/j.newast.2017.01.008
52. F. Coti Zelati, A. Papitto, D. de Martino, et al., *A&A*, **622**, A211 (2019). DOI 10.1051/0004-6361/201834835
53. D.F. Torres, L. Ji, J. Li, et al., *ApJ*, **836**(1), 68 (2017). DOI 10.3847/1538-4357/836/1/68
54. C. Ferrigno, E. Bozzo, A. Papitto, et al., *A&A*, **567**, A77 (2014). DOI 10.1051/0004-6361/201322904
55. S. Bogdanov, A.T. Deller, J.C.A. Miller-Jones, et al., *ApJ*, **856**(1), 54 (2018). DOI 10.3847/1538-4357/aaaeb9
56. A. Papitto, F. Ambrosino, L. Stella, et al., *ApJ*, **882**(2), 104 (2019). DOI 10.3847/1538-4357/ab2fdf
57. H.E. Bond, R.L. White, R.H. Becker, M.S. O'Brien, *PASP*, **114**(802), 1359 (2002). DOI 10.1086/344381
58. P. Szkody, O. Fraser, N. Silvestri, et al., *AJ*, **126**(3), 1499 (2003). DOI 10.1086/377346
59. Z. Wang, A.M. Archibald, J.R. Thorstensen, et al., *ApJ*, **703**(2), 2017 (2009). DOI 10.1088/0004-637X/703/2/2017
60. P.A. Woudt, B. Warner, M.L. Pretorius, *MNRAS*, **351**(3), 1015 (2004). DOI 10.1111/j.1365-2966.2004.07843.x
61. X. Wang, Z. Wang, N. Morrell, *ApJ*, **764**(2), 144 (2013). DOI 10.1088/0004-637X/764/2/144
62. J.P. Halpern, E. Gaidos, A. Sheffield, et al., *ATel* **5514**, 1 (2013)
63. A. Patruno, A.M. Archibald, J.W.T. Hessels, et al., *ApJ*, **781**(1), L3 (2014). DOI 10.1088/2041-8205/781/1/L3
64. D. Eckert, M. Del Santo, A. Bazzano, et al., *ATel* **4925**, 1 (2013)
65. S. Bégin, A search for fast pulsars in globular clusters. Master's thesis, University of British Columbia (2006)
66. M. Linares, A. Bahramian, C. Heinke, et al., *MNRAS*, **438**(1), 251 (2014). DOI 10.1093/mnras/stt2167
67. S.Y. Sazonov, M.G. Revnivtsev, *A&A*, **423**, 469 (2004). DOI 10.1051/0004-6361:20047150
68. N. Masetti, L. Morelli, E. Palazzi, et al., *A&A*, **459**(1), 21 (2006). DOI 10.1051/0004-6361:20066055
69. M.L. Pretorius, *MNRAS*, **395**(1), 386 (2009). DOI 10.1111/j.1365-2966.2009.14521.x
70. D. de Martino, M. Falanga, J.M. Bonnet-Bidaud, T. Belloni, et al., *A&A*, **515**, A25 (2010). DOI 10.1051/0004-6361/200913802
71. D. de Martino, T. Belloni, M. Falanga, et al., *A&A*, **550**, A89 (2013). DOI 10.1051/0004-6361/201220393
72. K. Saitou, M. Tsujimoto, K. Ebisawa, M. Ishida, *PASJ*, **61**, L13 (2009). DOI 10.1093/pasj/61.4.L13
73. A.B. Hill, A. Szostek, S. Corbel, et al., *MNRAS*, **415**(1), 235 (2011). DOI 10.1111/j.1365-2966.2011.18692.x
74. C. Thompson, R.D. Blandford, C.R. Evans, E.S. Phinney, *ApJ*, **422**, 304 (1994). DOI 10.1086/173728

75. J.W. Broderick, R.P. Fender, R.P. Breton, et al., *MNRAS*, **459**(3), 2681 (2016). DOI 10.1093/mnras/stw794
76. J.H. Applegate, J. Shaham, *ApJ*, **436**, 312 (1994). DOI 10.1086/174906
77. G. Voisin, R.P. Breton, C. Summers, *MNRAS*, **492**(2), 1550 (2020). DOI 10.1093/mnras/stz3430
78. O. McConnell, P.J. Callanan, M. Kennedy, et al., *MNRAS*, **451**(4), 3468 (2015). DOI 10.1093/mnras/stv1197
79. M.C. Baglio, P. D’Avanzo, S. Campana, et al., *A&A*, **591**, A101 (2016). DOI 10.1051/0004-6361/201628383
80. R.P. Breton, M.H. van Kerkwijk, M.S.E. Roberts, et al., *ApJ*, **769**(2), 108 (2013). DOI 10.1088/0004-637X/769/2/108
81. R.W. Romani, N. Sanchez, *ApJ*, **828**(1), 7 (2016). DOI 10.3847/0004-637X/828/1/7
82. F. Coti Zelati, M.C. Baglio, S. Campana, et al., *MNRAS*, **444**(2), 1783 (2014). DOI 10.1093/mnras/stu1552
83. S. Bogdanov, A.M. Archibald, C. Bassa, et al., *ApJ*, **806**(2), 148 (2015). DOI 10.1088/0004-637X/806/2/148
84. A. Papitto, N. Rea, F. Coti Zelati, et al., *ApJ*, **858**(2), L12 (2018). DOI 10.3847/2041-8213/aabee9
85. M.R. Kennedy, C.J. Clark, G. Voisin, R.P. Breton, *MNRAS*, **477**(1), 1120 (2018). DOI 10.1093/mnras/sty731
86. L. Homer, P. Szkody, B. Chen, et al., *AJ*, **131**(1), 562 (2006). DOI 10.1086/498346
87. A.M. Archibald, V.M. Kaspi, S. Bogdanov, et al., *ApJ*, **722**(1), 88 (2010). DOI 10.1088/0004-637X/722/1/88
88. S. Bogdanov, A.M. Archibald, J.W.T. Hessels, et al., *ApJ*, **742**(2), 97 (2011). DOI 10.1088/0004-637X/742/2/97
89. S.P. Tendulkar, C. Yang, H. An, et al., *ApJ*, **791**(2), 77 (2014). DOI 10.1088/0004-637X/791/2/77
90. K.L. Li, A.K.H. Kong, J. Takata, et al., *ApJ*, **797**(2), 111 (2014). DOI 10.1088/0004-637X/797/2/111
91. S. Bogdanov, A. Patruno, A.M. Archibald, et al., *ApJ*, **789**(1), 40 (2014). DOI 10.1088/0004-637X/789/1/40
92. S. Bogdanov, M. van den Berg, M. Servillat, C.O. Heinke, et al., *ApJ*, **730**(2), 81 (2011). DOI 10.1088/0004-637X/730/2/81
93. M. Linares, *ApJ*, **795**(1), 72 (2014). DOI 10.1088/0004-637X/795/1/72
94. M.S.E. Roberts, H. Al Noori, R.A. Torres, et al., in *Pulsar Astrophysics the Next Fifty Years, IAU Symposium*, vol. 337, ed. by P. Weltevrede, B.B.P. Perera, L.L. Preston, S. Sanidas (2018), *IAU Symposium*, vol. 337, pp. 43–46. DOI 10.1017/S1743921318000480
95. J. Arons, M. Tavani, *ApJ*, **403**, 249 (1993). DOI 10.1086/172198
96. H. Al Noori, M.S.E. Roberts, R.A. Torres, et al., *ApJ*, **861**(2), 89 (2018). DOI 10.3847/1538-4357/aac828
97. D. Kandel, R.W. Romani, H. An, *ApJ*, **879**(2), 73 (2019). DOI 10.3847/1538-4357/ab24d9
98. G. Dubus, A. Lamberts, S. Fromang, *A&A*, **581**, A27 (2015). DOI 10.1051/0004-6361/201425394
99. A. Possenti, R. Cerutti, M. Colpi, S. Mereghetti, *A&A*, **387**, 993 (2002). DOI 10.1051/0004-6361:20020472
100. V.E. Zavlin, *ApSS*, **308**(1-4), 297 (2007). DOI 10.1007/s10509-007-9297-y
101. A. Papitto, D. de Martino, T.M. Belloni, et al., *MNRAS*, **449**, L26 (2015). DOI 10.1093/mnras/ltv013
102. D.F. Torres, J. Li, arXiv e-prints arXiv:2004.03128 (2020)
103. P.H.T. Tam, C.Y. Hui, R.H.H. Huang, et al., *ApJ*, **724**(2), L207 (2010). DOI 10.1088/2041-8205/724/2/L207
104. P.L. Nolan, et al., *ApJS*, **199**(2), 31 (2012). DOI 10.1088/0067-0049/199/2/31
105. J. Takata, K.L. Li, G.C.K. Leung, et al., *ApJ*, **785**(2), 131 (2014). DOI 10.1088/0004-637X/785/2/131

106. T.J. Johnson, P.S. Ray, J. Roy, et al., *ApJ*, **806**(1), 91 (2015). DOI 10.1088/0004-637X/806/1/91
107. Y. Xing, Z. Wang, *ApJ*, **808**(1), 17 (2015). DOI 10.1088/0004-637X/808/1/17
108. V. De Falco, L. Kuiper, E. Bozzo, et al., *A&A*, **603**, A16 (2017). DOI 10.1051/0004-6361/201730600
109. M.M. Romanova, G.V. Ustyugova, A.V. Koldoba, R.V.E. Lovelace, *ApJ*, **616**(2), L151 (2004). DOI 10.1086/426586
110. R. Wijnands, N. Degenaar, D. Page, *JApA* **38**(3), 49 (2017). DOI 10.1007/s12036-017-9466-5
111. S. Campana, L. Stella, F. Gastaldello, et al., *ApJ*, **575**(1), L15 (2002). DOI 10.1086/342505
112. C.O. Heinke, P.G. Jonker, R. Wijnands, et al., *ApJ*, **691**(2), 1035 (2009). DOI 10.1088/0004-637X/691/2/1035
113. L. Burderi, T. Di Salvo, F. D’Antona, et al., *A&A*, **404**, L43 (2003). DOI 10.1051/0004-6361:20030669
114. S. Campana, P. D’Avanzo, J. Casares, et al., *ApJ*, **614**(1), L49 (2004). DOI 10.1086/425495
115. P. D’Avanzo, S. Campana, J. Casares, et al., *A&A*, **508**(1), 297 (2009). DOI 10.1051/0004-6361/200810249
116. J.M. Hartman, A. Patruno, D. Chakrabarty, et al., *ApJ*, **675**(2), 1468 (2008). DOI 10.1086/527461
117. T. Di Salvo, L. Burderi, A. Riggio, et al., *MNRAS*, **389**(4), 1851 (2008). DOI 10.1111/j.1365-2966.2008.13709.x
118. A. Patruno, A. Jaodand, L. Kuiper, et al., *ApJ*, **841**(2), 98 (2017). DOI 10.3847/1538-4357/aa6f5b
119. E. de Oña Wilhelmi, A. Papitto, J. Li, et al., *MNRAS*, **456**(3), 2647 (2016). DOI 10.1093/mnras/stv2695
120. M. Burgay, L. Burderi, A. Possenti, N. D’Amico, et al., *ApJ*, **589**(2), 902 (2003). DOI 10.1086/374690
121. M.N. Iacolina, M. Burgay, L. Burderi, et al., *A&A*, **497**(2), 445 (2009). DOI 10.1051/0004-6361/200810677
122. M.N. Iacolina, M. Burgay, L. Burderi, et al., *A&A*, **519**, A13 (2010). DOI 10.1051/0004-6361/201014025
123. S. Campana, F. Coti Zelati, A. Papitto, et al., *A&A*, **594**, A31 (2016). DOI 10.1051/0004-6361/201629035
124. F. Coti Zelati, S. Campana, V. Braitto, et al., *A&A*, **611**, A14 (2018). DOI 10.1051/0004-6361/201732244
125. A. Miraval Zanon, S. Campana, A. Ridolfi, et al., *A&A*, **635**, A30 (2020). DOI 10.1051/0004-6361/201936356
126. T. Shahbaz, M. Linares, S.P. Nevado, et al., *MNRAS*, **453**(4), 3461 (2015). DOI 10.1093/mnras/stv1686
127. T. Shahbaz, Y. Dallilar, A. Garner, S. Eikenberry, et al., *MNRAS*, **477**(1), 566 (2018). DOI 10.1093/mnras/sty562
128. M.C. Baglio, F. Vincentelli, S. Campana, et al., *A&A*, **631**, A104 (2019). DOI 10.1051/0004-6361/201936008
129. J.V. Hernandez Santisteban, Unravelling the nature of transitional millisecond pulsars. Ph.D. thesis, University of Amsterdam (2019)
130. J.H.K. Wu, C.Y. Hui, E.M.H. Wu, et al., *ApJ*, **765**(2), L47 (2013). DOI 10.1088/2041-8205/765/2/L47
131. Y. Xing, Z.X. Wang, J. Takata, *RAA* **18**(10), 127 (2018). DOI 10.1088/1674-4527/18/10/127
132. E. Aliu, et al., *ApJ*, **831**(2), 193 (2016). DOI 10.3847/0004-637X/831/2/193
133. E. Gallo, N. Degenaar, J. van den Eijnden, *MNRAS*, **478**(1), L132 (2018). DOI 10.1093/mnrasl/sly083
134. A. Bahramian, J. Strader, L. Chomiuk, et al., *ApJ*, **864**(1), 28 (2018). DOI 10.3847/1538-4357/aad68b
135. A.T. Deller, J. Moldon, J.C.A. Miller-Jones, et al., *ApJ*, **809**(1), 13 (2015). DOI 10.1088/0004-637X/809/1/13

136. R. Fender, *Astronomische Nachrichten* **337**(4-5), 381 (2016). DOI 10.1002/asna.201612317
137. J.P. Halpern, E. Gaidos, A. Sheffield, et al., *ATel* **5514**, 1 (2013)
138. P. Hakala, J.J.E. Kajava, *MNRAS*, **474**(3), 3297 (2018). DOI 10.1093/mnras/stx2922
139. J.V. Hernandez Santisteban, Multi-wavelength Observations of Accreting Compact Objects. Ph.D. thesis, University of Southampton (2016)
140. K. Saitou, M. Tsujimoto, K. Ebisawa, et al., *PASJ*, **63**, S759 (2011). DOI 10.1093/pasj/63.sp3.S759
141. A.M. Archibald, S. Bogdanov, A. Patruno, et al., *ApJ*, **807**(1), 62 (2015). DOI 10.1088/0004-637X/807/1/62
142. F. Ambrosino, A. Papitto, L. Stella, et al., *Nature Astronomy* **1**, 854 (2017). DOI 10.1038/s41550-017-0266-2
143. L. Zampieri, A. Burtovoi, M. Fiori, et al., *MNRAS*, **485**(1), L109 (2019). DOI 10.1093/mnras/slz043
144. S. Karpov, G. Beskin, V. Plokhhotnichenko, et al., *AN* **340**(7), 607 (2019). DOI 10.1002/asna.201913663
145. A. Burtovoi, L. Zampieri, M. Fiori, et al., *MNRAS*, (2020). DOI 10.1093/mnras/slaa133
146. N. Masetti, B. Sbarufatti, P. Parisi, et al., *A&A*, **559**, A58 (2013). DOI 10.1051/0004-6361/201322611
147. S. Bogdanov, J.P. Halpern, *ApJ*, **803**(2), L27 (2015). DOI 10.1088/2041-8205/803/2/L27
148. S. Bogdanov, *ApJ*, **826**(1), 28 (2016). DOI 10.3847/0004-637X/826/1/28
149. C.T. Britt, J. Strader, L. Chomiuk, et al., *ApJ*, **849**(1), 21 (2017). DOI 10.3847/1538-4357/aa8e41
150. Gaia Collaboration, *A&A*, **616**, A14 (2018). DOI 10.1051/0004-6361/201832916
151. C.A.L. Bailer-Jones, J. Rybizki, M. Fouesneau, et al., *AJ*, **156**(2), 58 (2018). DOI 10.3847/1538-3881/aacb21
152. J.A. Tomsick, S. Chaty, J. Rodriguez, et al., *ApJ*, **701**(1), 811 (2009). DOI 10.1088/0004-637X/701/1/811
153. J.M. Miller, S.J. Swihart, J. Strader, et al., arXiv e-prints arXiv:2009.09054 (2020)
154. J. Strader, K.L. Li, L. Chomiuk, et al., *ApJ*, **831**(1), 89 (2016). DOI 10.3847/0004-637X/831/1/89
155. M.R. Kennedy, R.P. Breton, C.J. Clark, et al., *MNRAS*, **494**(3), 3912 (2020). DOI 10.1093/mnras/staa912
156. K.L. Li, J. Strader, J.C.A. Miller-Jones, et al., *ApJ*, **895**(2), 89 (2020). DOI 10.3847/1538-4357/ab8f28
157. S. Abdollahi, et al., *ApJS*, **247**(1), 33 (2020). DOI 10.3847/1538-4365/ab6bcb
158. J. Ballet, T.H. Burnett, S.W. Digel, B. Lott, arXiv e-prints arXiv:2005.11208 (2020)
159. N. Rea, F. Coti Zelati, P. Esposito, et al., *MNRAS*, **471**(3), 2902 (2017). DOI 10.1093/mnras/stx1560
160. J.P. Halpern, S. Bogdanov, J.R. Thorstensen, *ApJ*, **838**(2), 124 (2017). DOI 10.3847/1538-4357/838/2/124
161. P.B. Cho, J.P. Halpern, S. Bogdanov, *ApJ*, **866**(1), 71 (2018). DOI 10.3847/1538-4357/aade92
162. M.M. Romanova, S.P. Owocki, *SSRv* **191**(1-4), 339 (2015). DOI 10.1007/s11214-015-0200-9
163. S.J. Swihart, J. Strader, T.J. Johnson, et al., *ApJ*, **851**(1), 31 (2017). DOI 10.3847/1538-4357/aa9937
164. S.J. Swihart, J. Strader, L. Shishkovsky, et al., *ApJ*, **866**(2), 83 (2018). DOI 10.3847/1538-4357/aadcab
165. Z. Wang, Y. Xing, J. Zhang, K. Boutsia, et al., *MNRAS*, **493**(4), 4845 (2020). DOI 10.1093/mnras/staa655
166. C.O. Heinke, A. Bahramian, N. Degenaar, R. Wijnands, *MNRAS*, **447**(4), 3034 (2015). DOI 10.1093/mnras/stu2652
167. N. Degenaar, R. Wijnands, M.T. Reynolds, et al., *ApJ*, **792**(2), 109 (2014). DOI 10.1088/0004-637X/792/2/109
168. N. Degenaar, R. Wijnands, J.M. Miller, et al., *JHEAp* **7**, 137 (2015). DOI 10.1016/j.jheap.2015.03.005

169. A. Bahramian, J. Strader, J.C.A. Miller-Jones, et al., arXiv e-prints arXiv:2007.04581 (2020)
170. M. Tavani, *ApJ*, **379**, L69 (1991). DOI 10.1086/186156
171. J. Lee, C.Y. Hui, J. Takata, et al., *ApJ*, **864**(1), 23 (2018). DOI 10.3847/1538-4357/aad284
172. A.K.H. Kong, C.Y. Hui, J. Takata, et al., *ApJ*, **839**(2), 130 (2017). DOI 10.3847/1538-4357/aa6aa2
173. L. Sironi, U. Keshet, M. Lemoine, *SSRv* **191**(1-4), 519 (2015). DOI 10.1007/s11214-015-0181-8
174. S. Bogdanov, J.E. Grindlay, M. van den Berg, *ApJ*, **630**(2), 1029 (2005). DOI 10.1086/432249
175. Z. Wadiasingh, A.K. Harding, C. Venter, et al., *ApJ*, **839**(2), 80 (2017). DOI 10.3847/1538-4357/aa69bf
176. Z. Wadiasingh, C. Venter, A.K. Harding, et al., *ApJ*, **869**(2), 120 (2018). DOI 10.3847/1538-4357/aaed43
177. N. Sanchez, R.W. Romani, *ApJ*, **845**(1), 42 (2017). DOI 10.3847/1538-4357/aa7a02
178. D.F. Torres, *NatAs* **2**, 247 (2018). DOI 10.1038/s41550-018-0384-5
179. D.F. Torres, D. Viganò, F. Coti Zelati, J. Li, *MNRAS*, **489**(4), 5494 (2019). DOI 10.1093/mnras/stz2403
180. M.M. Romanova, A.A. Blinova, G.V. Ustyugova, et al., *NewA*, **62**, 94 (2018). DOI 10.1016/j.newast.2018.01.011
181. A. Papitto, D.F. Torres, J. Li, *MNRAS*, **438**(3), 2105 (2014). DOI 10.1093/mnras/stt2336
182. A. Papitto, D.F. Torres, *ApJ*, **807**(1), 33 (2015). DOI 10.1088/0004-637X/807/1/33
183. C.R. D'Angelo, H.C. Spruit, *MNRAS*, **416**(2), 893 (2011). DOI 10.1111/j.1365-2966.2011.19029.x
184. C.R. D'Angelo, H.C. Spruit, *MNRAS*, **420**(1), 416 (2012). DOI 10.1111/j.1365-2966.2011.20046.x
185. Ü. Ertan, *MNRAS*, **479**(1), L12 (2018). DOI 10.1093/mnras/sly089
186. K. Parfrey, A. Spitkovsky, A.M. Beloborodov, *ApJ*, **822**(1), 33 (2016). DOI 10.3847/0004-637X/822/1/33
187. K. Parfrey, A. Spitkovsky, A.M. Beloborodov, *MNRAS*, **469**(3), 3656 (2017). DOI 10.1093/mnras/stx950
188. S. Bhattacharyya, *MNRAS*, **498**(1), 728 (2020). DOI 10.1093/mnras/staa2304
189. B. Haskell, A. Patruno, *PhRvL* **119**(16), 161103 (2017). DOI 10.1103/PhysRevLett.119.161103
190. A. Veledina, J. Nättilä, A.M. Beloborodov, *ApJ*, **884**(2), 144 (2019). DOI 10.3847/1538-4357/ab44c6
191. S.V. Bogovalov, *A&A*, **349**, 1017 (1999)
192. S. Campana, A. Miraval Zanon, F. Coti Zelati, et al., *A&A*, **629**, L8 (2019). DOI 10.1051/0004-6361/201936312
193. K. Parfrey, A. Tchekhovskoy, *ApJ*, **851**(2), L34 (2017). DOI 10.3847/2041-8213/aa9c85
194. K.Y. Ekşil, M.A. Alpar, *ApJ*, **620**(1), 390 (2005). DOI 10.1086/425959
195. J.P. Lasota, *NewAR*, **45**(7), 449 (2001). DOI 10.1016/S1387-6473(01)00112-9
196. S. van Straaten, M. van der Klis, R. Wijnands, *ApJ*, **619**(1), 455 (2005). DOI 10.1086/426183
197. Y.E. Lyubarskii, *MNRAS*, **292**(3), 679 (1997). DOI 10.1093/mnras/292.3.679